

Synthesis, Optical and Morphological Characterization of PbSe Quantum Dots for Diagnostic Studies: A model Study

A dissertation submitted in fulfillment of the requirements for the degree

Master of Science

In

Chemistry

Department of Chemistry



UNIVERSITY *of the*
WESTERN CAPE

Immaculate Linda Achieng' Ouma
BSc Chemistry (University of Nairobi)

Supervisors: Dr. Martin Onani
Dr. Abram Madiehe

KEYWORDS

PbSe

Quantum dots (QDs)

Semiconductor nanocrystals (NCs)

Near-infrared (NIR)

Organometallic synthesis

Aqueous synthesis

Ligand exchange

Photoluminescence spectroscopy (PL)

Energy-dispersive X-ray spectroscopy (EDS)

3-Mercaptopropionic acid (MPA)

11-Mercaptoundecanoic acid (MUA)

Water-soluble tetrazolium salt (WST-1)



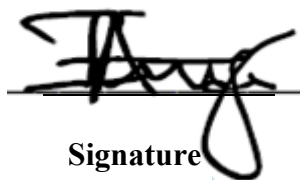
ABSTRACT

In this study PbSe quantum dots (QDs) were successfully synthesized via the organometallic and aqueous routes. Optical characterization was carried out using photoluminescence (PL) spectroscopy, structural and morphological characterization were carried out using X-ray diffraction (XRD) and transmission electron microscopy (TEM). Energy-dispersive X-ray spectroscopy (EDS) was used to determine the composition of the QDs. All the synthesized QDs were found to have emissions within the near-infrared region of the spectrum (≥ 1000 nm) with most of them being less than 5 nm in size. The aqueous synthesized QDs had a perfect Gaussian emission spectrum with a FWHM of ~ 23 nm indicating pure band gap emission and narrow size distribution respectively. The QDs were determined to have a cubic rock-salt crystal structure consistent with bulk PbSe. The aqueous synthesized QDs were however not stable in solution with the QDs precipitating after approximately 48 h. The organometallic synthesized QDs were transferred into the aqueous phase by exchanging the surface oleic acid ligands with 11-mercaptoundecanoic acid ligands. The ligand exchanged QDs were however stable in solution for over two weeks. The effects of reaction parameters on the optical and structural properties of the organometallic synthesized QDs were investigated by varying the reaction time, temperature, ligand purity, lead and selenium sources. It was observed that larger QDs were formed with longer reaction times, with reactions proceeding faster at higher reaction temperatures than at lower temperatures. Varying the ligand purity was found to have minimal effects on the properties of the synthesized QDs. The lead and selenium sources contributed largely to the properties of the QDs with lead oxide producing spherical QDs which were smaller compared to the cubic QDs produced from lead acetate. TBPSe was seen to produce smaller QDs as compared to TOPSe. The cytotoxicity of the synthesized QDs was determined following the WST-1 cell viability assay with the QDs being found to be non-toxic at all the tested concentrations.

DECLARATION

I declare that **Synthesis, Optical and Morphological Characterization of PbSe Quantum Dots for Diagnostic Studies: A Model Study** is my own work, that it has not been submitted for any degree or examination in any other university, and that all the sources I have used or quoted have been indicated and acknowledged by complete references.

Immaculate Linda Achieng' Ouma



Signature



03rd March 2014

Date

DEDICATION



ACKNOWLEDGEMENTS

I wish to express my sincere gratitude to all the people without whose help this work would not have been a success.

First I thank the Almighty God for his grace which has been abundant in my life thus far.

I greatly appreciate the guidance of my supervisors who guided me throughout the course of this work to its successful completion. My sincere gratitude goes to Dr. Paul Mushonga for all the time spent guiding and advising me on the path to take may God richly bless you. My colleagues in the organometallic research lab who worked alongside me, your encouragement as we walked and worked together is highly appreciated.

I wish to thank Ms. Nicole Sibuyi who patiently assisted me in the course of my biological assays without ever tiring, I deeply grateful to you my friend. Many thanks to the sensor lab team for allowing me access to the NanoLog instrument and Dr. Subelia Botha of the EMU for carrying out TEM analysis of my samples. I would also like to thank all my friends and colleagues who in their special ways contributed to the success of this work.

Much appreciation goes to the University of the Western Cape for offering me an opportunity to join this wonderful family of friends and colleagues and providing the facilities to carry out this work. To the staff of the department of chemistry for assisting me throughout the course of my studies I am truly grateful.

I also wish to thank DST/Mintek Nanotechnology innovation center who through the biolabels node director Dr. Mervin Meyer provided the funds to carry out this work.

Finally my deepest gratitude goes to my family members whose love and support helped me hold on to the end.

CONFERENCE CONTRIBUTIONS AND PUBLICATIONS

Conference contributions

1. **Immaculate L.A. Ouma**, Paul Mushonga, Martin O. Onani, Abram M. Madiehe, Mervin Meyer. *Synthesis, optical and morphological characterization of doped PbX/PbS (X = Se, Te) quantum dots for diagnostic Studies: a model study*. 1st Pan-African Summer School in Nanomedicine. Pretoria, South Africa. 3rd – 11th Nov 2012. **Poster presentation.**
2. **Immaculate L.A. Ouma**, Paul Mushonga, Abram M. Madiehe, Mervin Meyer, Martin O. Onani, Francis B. Dejene. *Synthesis and characterization of near-infrared emitting PbSe quantum dots*. 5th South African Conference on Photonic Materials (SACPM). Kariega game reserve, South Africa. 29th April - 3rd May 2013. **Poster presentation.**
3. **Immaculate L.A. Ouma**, Paul Mushonga, Abram M. Madiehe, Mervin Meyer, Martin O. Onani, Francis B. Dejene. *Synthesis and characterization of MPA-capped PbSe nanocrystals*. UWC Postgraduate Research Open Day, University of the Western Cape, South Africa. 30th Oct 2013. **Poster presentation.**
4. **Immaculate L.A. Ouma**, Paul Mushonga, Abram M. Madiehe, Mervin Meyer, Martin O. Onani, Francis B. Dejene. *Size and shape evolution of Lead salt Nanocrystals*. PACN congress on sustainability in Africa. Energy, water and waste, Addis Ababa, Ethiopia. 3th - 5th Dec 2013. **Oral presentation.**
5. **Immaculate L.A. Ouma**, Paul Mushonga, Abram M. Madiehe, Mervin Meyer, Francis B. Dejene, Martin O. Onani, 2013. *Effect of reaction parameters on the growth and optical properties of PbSe nanocrystals*. The 7th International Conference of the Africa Materials Research Society. Addis Ababa, Ethiopia. 8th - 13th Dec 2013. **Oral presentation.**

Publications

1. **Immaculate L.A. Ouma**, Paul Mushonga, Abram M. Madiehe, Mervin Meyer, Francis B. Dejene, Martin O. Onani. *Synthesis, optical and morphological characterization of MPA-capped PbSe nanocrystals*. Physica B: Condensed Matter. <http://dx.doi.org/10.1016/j.physb.2013.10.057>.

TABLE OF CONTENTS

KEYWORDS	ii
ABSTRACT	iii
DECLARATION	iv
DEDICATION	v
ACKNOWLEDGEMENTS	vi
CONFERENCE CONTRIBUTIONS AND PUBLICATIONS	vii
ABBREVIATIONS AND SYMBOLS	xii
LIST OF TABLES	xiv
LIST OF FIGURES	xv
LIST OF SCHEMES	xvii
CHAPTER 1	1
1 Introduction	1
1.1 Nanotechnology	1
1.2 Quantum dots (QDs)	4
1.2.1 Group IV-VI Nanocrystals.....	5
1.3 QD synthesis	6
1.3.1 Aqueous synthesis.....	7
1.3.2 Organometallic synthesis	7
1.3.2.1 Hot injection technique	8
1.3.2.2 Heating-up technique	10
1.4 Ostwald ripening.....	11
1.5 Surface modification	12
1.5.1 Aqueous solubilization.....	12
1.5.1.1 Ligand Exchange	13

1.5.1.2 Amphiphilic polymer encapsulation	17
1.6 Application of QDs in diagnostic studies.....	19
1.6.1 Near-infrared (NIR) QDs	20
1.7 Problem statement.....	22
1.8 Aims and objectives	23
1.9 References	24
CHAPTER 2.....	30
2 Experimental.....	30
2.1 Materials.....	30
2.2 Instrumentation	30
2.2.1 Photoluminescence spectroscopy (PL)	30
2.2.2 X-ray diffraction (XRD).....	32
2.2.3 Transmission electron microscopy (TEM)	32
2.3 Synthesis and purification of PbSe QDs	33
2.3.1 Organometallic reactions	34
2.3.1.1 Preparation of reaction precursors	34
2.3.1.1.1 Preparation of Lead precursor	34
2.3.1.1.2 Preparation of chalcogen precursor	34
2.3.1.2 Preparation of PbSe QDs	34
2.3.1.3 Purification of QDs	35
2.3.1.4 Ligand Exchange	35
2.3.1.4.1 3-Mercaptopropionic acid (MPA) ligands.....	35
2.3.1.4.2 11-Mercaptoundecanoic acid (MUA) ligands	36
2.3.1.5 Investigation of the effects of reaction parameters on the optical and structural properties of PbSe QDs.....	36
2.3.2 Aqueous reactions	38
2.3.2.1 Preparation of Lead precursor.....	38
2.3.2.2 Preparation of selenium precursor	38
2.3.2.3 Synthesis of MPA-capped PbSe QDs	38
2.3.2.4 Purification of QDs	39

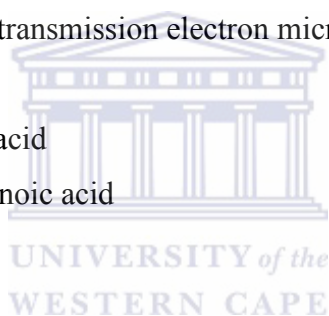
2.4 Cytotoxicity experiments	39
2.5 References	41
CHAPTER 3.....	42
3 Results and discussion	42
3.1 Synthesis of PbSe QDs in organic media.....	42
3.1.1 Effect of temperature on the optical properties of PbSe QDs.....	43
3.1.2 Solvent effects on the optical and structural properties of PbSe QDs	51
3.1.3 Effect of ligand purity on the optical and structural properties of PbSe QDs	54
3.1.4 Effect of Lead and Selenium sources on the optical and structural properties of PbSe QDs	56
3.1.4.1 Summary of the effects of lead and selenium sources on the optical and structural properties of PbSe QDs.....	59
3.2 Ligand exchange of organic synthesized QDs	60
3.3 Synthesis of PbSe QDs in aqueous media	62
3.3.1 Photoluminescence properties.....	63
3.3.2 Structural properties	64
3.3.2.1 Transmission electron microscopy	64
3.3.2.2 X-ray diffraction patterns.....	67
3.4 References	68
CHAPTER 4.....	71
4 Biological applications of PbSe quantum dots	71
4.1 Results of preliminary cytotoxicity studies.....	71
4.2 References	74
CHAPTER 5.....	75
5 Conclusions and recommendations.....	75
5.1 Conclusions.....	75
5.2 Recommendations	76

5.3 References.....78



ABBREVIATIONS AND SYMBOLS

°C	Degrees Celsius
AAS	Atomic absorption spectroscopy
DHLA	Dihydrolipoic acid
DPP	Diphenylphosphine
EDS	Energy-dispersive X-ray spectroscopy
eV	Electron volt
FRET	Fluorescence Resonance Energy Transfer
FWHM	full width at half maximum
g	Gram
h	Hour
HRTEM	High resolution transmission electron microscopy
L	Litre
MAA	Mercaptoacetic acid
MHA	6-Mercaptohexanoic acid
min	Minute
mL	Milliliter
mmol	Millimoles
mol	Mole
MPA	3-Mercaptopropionic acid
MUA	11-Mercaptoundecanoic acid
NC	Nanocrystal
nm	Nanometer
NP	Nanoparticles
ODE	1-Octadecene
OLA	Oleylamine
PBS	Phosphate buffered saline
PEG	Polyethylene glycol
PL	Photoluminescence
QCE	Quantum confinement effect
QD	Quantum dot



QY	Quantum Yield
rpm	revolutions per minute
SAED	Selected area electron diffraction
SWCNT	Single walled carbon nanotubes
TBP	Tributylphosphine
TEM	Transmission electron microscope
TGA	Thioglycolic acid
TOP	Trioctylphosphine
TOPO	Trioctylphosphine oxide
UV	Ultraviolet
WST-1	Water-soluble tetrazolium salt
XRD	X-ray Diffraction
μL	Microliter



LIST OF TABLES

Table 1.1	Some Mercaptocarboxylic acids used in ligand exchange reactions	15
Table 1.2	Representation of QD aqueous solubilization and biofunctionalization strategies. Ligands provide linkage to QD (pink), water solubility (blue) and a biomolecule linking functionality.....	18
Table 2.1	Effect of injection temperature and growth time	37
Table 2.2	Effect of solvent.....	37
Table 2.3	Effect of lead and selenium sources.....	37
Table 2.4	Effect of ligand purity	37
Table 3.1	Effect of ligand purity on the optical and structural properties of PbSe QDs.	56
Table 3.2	Effect of lead and selenium sources on the optical and structural properties of PbSe QDs.	60



LIST OF FIGURES

Figure 1.1	Representation of Ostwald ripening	11
Figure 1.2	Ligand exchange of oleic acid capped PbSe QDs with monodentate and bidentate thiol ligands.....	16
Figure 1.3	Some QD materials and their emission wavelengths on the spectrum. Some of the areas of biological interest are also shown.. ..	20
Figure 2.1	Schematic representation of a Horiba Jobinyvon NanoLog, showing the optical path from source through sample to detectors.....	31
Figure 2.2	Tecnai™ Transmission electron microscope	33
Figure 3.1	PL spectra of PbSe QDs aliquots taken during synthesis at 90 °C.....	44
Figure 3.2	(A) TEM micrograph and (B) size distribution of PbSe QDs synthesized at 90 °C.....	45
Figure 3.3	PL spectra of PbSe QDs aliquots taken during synthesis at 120 °C.....	46
Figure 3.4	(A) TEM micrograph and (B) size distribution of PbSe QDs synthesized at 120 °C.....	46
Figure 3.5	PL spectra of PbSe QDs aliquots taken during synthesis at 150 °C.....	48
Figure 3.6	(A) TEM micrograph and (B) size distribution of PbSe QDs synthesized at 150 °C.....	48
Figure 3.7	Emission spectra of QDs synthesized at different reaction temperatures.....	50
Figure 3.8	Summary of emission maxima with time at different reaction temperatures....	51
Figure 3.9	Summary of emission maxima with time in different solvents	53
Figure 3.10	(A) TEM micrograph and (B) size distribution of PbSe QDs synthesized with TOP as solvent.....	53
Figure 3.11	(A) TEM micrograph and (B) size distribution of PbSe QDs synthesized with OLA as solvent	54
Figure 3.12	(A) TEM micrograph and (B) size distribution of PbSe QDs synthesized from PbO, TBPSe and 90 % oleic acid	55
Figure 3.13	(A) TEM micrograph and (B) size distribution of PbSe QDs synthesized from PbO, TBPSe and 99 % oleic acid	55
Figure 3.14	(A) TEM micrograph and (B) size distribution of PbSe QDs synthesized from PbO and TOPSe.....	58

Figure 3.15 (A) TEM micrograph and (B) size distribution of PbSe quantum dots synthesized from Pb(Ac) ₂ and TOPSe.....	58
Figure 3.16 (A) TEM micrograph and (B) size distribution of PbSe quantum dots synthesized from PbO and TBPSe.....	59
Figure 3.17 EDS spectrum of PbSe quantum dots.....	60
Figure 3.18 PL spectra of oleic acid-capped QDs (QD37-OA) and 11-mercaptoundecanoic acid-capped QDs (QD37-MUA) following ligand exchange.....	62
Figure 3.19 Normalized PL spectrum of MPA-capped PbSe QDs.....	64
Figure 3.20 (A) TEM micrograph and (B) High resolution TEM image showing lattice fringes.....	66
Figure 3.21 EDS spectrum of PbSe nanocrystals.....	66
Figure 3.22 X-Ray diffractogram of MPA capped PbSe QDs.....	67
Figure 4.1 Effects of PbSe QDs on Caco-2 cell viability.....	72



LIST OF SCHEMES

Scheme 1.1 Proposed mechanism for PbSe nanocrystal formation [41]	9
Scheme 1.2 Proposed mechanism for DPP mediated PbSe nanocrystal formation [41]	10



1 Introduction

1.1 Nanotechnology

Nanotechnology has attracted a lot of interest in various scientific disciplines due to its applications in several areas including optics, magnetics, electronics and biological imaging [1]. Nanotechnology generally refers to the manipulation of matter on an atomic or molecular scale [2]. It involves materials with at least one dimension on the scale of 1-100 nm. A nanometre is 10^{-9} metres; 1 nanometre is approximately the width of three atoms. The average human hair has been approximated to have a width of 25,000 nm [3]. Nanoparticles have widely been used to enable scientists explore some of the smallest units of matter with large surface area to volume ratios. In nanometer-scale structures, finite size effects give rise to novel electronic, magnetic and structural properties [4]. As the size of a semiconductor decreases, the continuous energy levels in the bulk semiconductor become discrete [5]. This leads to quantum confinement effects (QCE) defined by an increasing band gap accompanied by the quantization of the energy levels to discrete values [6]. Confining electrons to small spatial dimensions causes them to acquire kinetic energy i.e. confinement energy which causes their energy spectra to become discrete [7]. These energy level changes are as a result of an increase in the effective energy gap relative to the bulk material and the emergence of discrete exciton states [8]. When the size of the semiconductor is so small, the electron “feels” confined causing the continuous spectrum to split into smaller energy levels with gaps between each successive level becoming discrete and increasing the energy levels [7,8]. Thus, if the size of the nanoparticle is small enough that the quantum confinement effects (QCE) dominate (typically less than 10 nm), the electronic and optical properties change, and the fluorescence wavelength is determined by its size [9]. Quantum confinement effects can

be divided into weak, intermediate or strong confinement regimes based on the size relationship between the radius of the nanoparticle and the exciton (electron and hole pair) Bohr radius. The Bohr radii can be described by **Equation 1.1** below [8].

$$a_{e,h} = \frac{4\pi\epsilon(\infty)\hbar^2}{m_{e,h}e^2} \quad \text{Equation 1.1}$$

Where

a_e = electron Bohr radius

a_h = hole Bohr radius

$\epsilon(\infty)$ = optical frequency dielectric constant

m_e = electron effective mass

m_h = hole effective mass

e = elementary charge

\hbar = reduced Planck's constant ($h/2\pi$)



The nanoparticles that have radii larger than the exciton Bohr radius ($R > a_e, a_h$) are said to be in the 'weak confinement regime' where the electron and hole retain their bulk character and are unaffected by quantum confinement. In the intermediate confinement regime, the radius of the nanoparticle is smaller than the electron Bohr radius but larger than the hole Bohr radius ($a_e > R > a_h$). The electron experiences confinement while the hole experiences coulomb attraction to the electron. In the strong confinement regime, the radius of the nanoparticle is smaller than both the electron and hole Bohr radii ($R < a_e, a_h$). In this regime both the electron and hole experience strong quantum confinement leading to splitting of energy levels into discrete states [8]. Quantum confinement of both the electron and hole leads to an increase in the effective band gap of the material with decreasing nanocrystal size [10]. Quantum

confinement effects (of the first excited electronic state) can be described by **Equation 1.2** below [11].

$$E \sim E_g + \frac{\hbar^2 \pi^2}{2R^2} \left[\frac{1}{m_e} + \frac{1}{m_h} \right] - \frac{1.8e^2}{\epsilon R} \quad \text{Equation 1.2}$$

Where

E = energy gap of quantum dots

E_g = bulk energy gap

R = quantum dot radius

ϵ = semiconductor dielectric constant

m_e = electron effective mass

m_h = hole effective mass

e = elementary charge

\hbar = reduced Planck's constant ($h/2\pi$)

As the radius of the nanoparticle decreases, E shifts to higher energy due to higher quantum confinement which follows R^{-2} . The Coulomb term which follows R^{-1} shifts E to lower energy as R decreases [11,12]. This increase in nanocrystal energy with decrease in size can explain the optical properties of nanocrystals, as nanocrystal sizes decrease their absorbance shift to shorter wavelengths. This has been observed in solution phase synthesis [12] as well as in solid state pyrolysis of molecular precursors [13].

QCE also determines the fluorescence properties of semiconductor nanocrystals. The fluorescence of the nanocrystals is a result of exciting the valence electron with a certain energy (or wavelength) and the emission of lower energy in the form of photons as the excited electron returns to the ground state recombining with the hole. The energy of the emitted photon is determined by the size of the nanocrystal due to quantum confinement effects. In a simplified model of the excitation, the energy of the emitted photon can be seen

as a sum of the band gap energy between occupied level and unoccupied energy level, the confinement energies of the hole and the excited electron, and the bound energy of the exciton (the electron-hole pair) [14]. Group IV-VI semiconductors have relatively large Bohr radii which offer unique access to strong quantum confinement regime [15]. In PbSe the electron, hole and exciton Bohr radii are 23 nm, 23 nm and 46 nm respectively, these allow strong confinement to be achieved in relatively large particles [16-17].

1.2 Quantum dots (QDs)

Semiconductor nanocrystals (NCs) also referred to as quantum dots (QDs), are nanometre sized crystals made of atoms from groups II-VI, III-V, and IV-VI [18]. While quantum wells and quantum wires experience quantum confinement in one and two dimensions respectively, QDs experience these quantum confinement effects in all three dimensions [19]. Semiconductor QDs possess novel electronic, optical, magnetic, and structural properties which are quite different from those of bulk materials [20]. Most QDs consist of a semiconductor core which is surrounded by a covering of wide band gap semiconductor shell in order to minimize the surface deficiency and enhance the quantum yield (QY) [21]. Compared to plain core quantum dots, core/shell QDs offer an enhanced stability and tunability of the optical and electronic properties. This is due to the spatial distribution of electron and hole wave functions in the QD heterostructures [22]. Core/shell QDs can be classified into three regimes depending on the localization of the charge carrier wave functions. In type I localization regime, the electron and hole are both localized in the core resulting in chemically stable and well-passivated QDs with high photoluminescence (PL) and quantum yield (QY). In type-II regime, the electron and hole are spatially separated. In a quasi-type-II localization regime, one of the carriers is fully delocalized while the other remains localized [22].

1.2.1 Group IV-VI Nanocrystals

Semiconductor nanocrystals or quantum dots (QDs) from groups II-VI e.g. CdSe and III-V e.g. InP have been widely studied and found applicable in various biological systems [23]. These applications include molecular histopathology, disease diagnosis, biological imaging among others [21]. CdSe QDs have also been used in developing kits for western blot analysis [24]. Comparatively less is known about group IV-VI QDs, especially their applications in biological studies [17]. Studies of lead salt QDs were originally motivated by the possibility of achieving uniquely strong confinement of charge carriers, along with size-quantized optical transitions in the infrared region. They display ferroelectric effects, have large optical and dielectric constants and negative pressure coefficients [25]. Lead chalcogenides (PbS, PbSe and PbTe) have attracted interest due to their distinguished physical properties. These semiconductors have cubic (rock-salt) crystal structure, very narrow energy gaps (direct gaps at L point) of 0.29 eV, 0.27 eV, and 0.41 eV for PbS, PbSe and PbTe respectively [26]. They have very large Bohr radii (20-46 nm) as compared to cadmium systems (2-10 nm). These large Bohr radii permit the optical properties of lead chalcogenides to be evaluated in the limit of extremely strong quantum confinement due to the size dependent behavior of these crystals [16-17]. Lead chalcogenide QDs emit near infrared (NIR) light which makes them ideal for biological imaging since their emissions fall within the second biological window of wavelengths between 1000 nm and 1350 nm [17,27]. Their high nonlinearities also make them excellent materials for optical switches [17]. The lowest energy exciton transitions occur at technologically important infrared wavelengths making them advantageous for optical applications [16].

1.3 QD synthesis

Preparation of QD samples that are uniform in composition, size, shape, internal structure and surface chemistry is essential to successfully mapping their size-dependent material properties. Semiconductor quantum dots (QDs) have been synthesized using various methods over the past decades. Early fabrication of semiconductor quantum dots was carried out in polymers [28], silicate glass and phosphate glass [29]. Some reports have also been given of the preparation of nanometre sized particles by the pyrolysis of molecular precursors. However, these methods were not able to produce QDs with uniform size distributions [13]. A great breakthrough in the colloidal synthesis of QDs was made by Murray and co-workers when they made use of trialkylphosphine chalcogenides in the synthesis of Cd-chalcogenide QDs [30]. In these reactions, dialkyl-metal compounds were used as the metal precursors while trialkylphosphine chalcogenides and silyl-chalcogenides were used as chalcogenide precursors [30-31]. These reactions provided the much needed size control during QD synthesis which had previously been difficult to achieve. This synthetic technique has since been modified replacing the dialkyl-metal compounds with other environmentally friendly metal precursors. Metal oxides and other metal salts have been used together with organic ligands in coordinating or noncoordinating solvents. Solution phase or colloidal synthesis can be carried out in organic or aqueous media. The semiconductor QDs produced consists of an inorganic core surrounded by an outer layer of organic surfactant molecules [32]. Depending on the surfactant molecules, the synthesized semiconductor QDs are soluble either in aqueous or organic media.

Although the pioneering work was done in organic solvents, aqueous synthetic protocols have since been developed for most semiconductor QDs. The synthesis can therefore be subdivided into organometallic and aqueous synthesis.

1.3.1 Aqueous synthesis

Synthesis of QDs in aqueous media provides nanoparticles which are compatible with biological environments. These syntheses are carried out using phosphates or thiols acting as stabilizing agents in aqueous media [33]. Aqueous synthesis for CdTe QDs in the presence of a thiol stabilizer was reported by Gaponik *et al.* in 2002 [34]. Most aqueous synthesis methods have focused on group II-VI nanocrystals. Yu *et al.* investigated the aqueous synthesis of dihydrolipoic acid (DHLLA) capped PbSe QDs. They reported on the optical and morphological properties of the as-synthesized QDs. QD growth was observed to be consistent with the widely investigated organometallic techniques with QD sizes increasing with growth time and Ostwald ripening also taking place in these systems [35]. Recently, the first room temperature aqueous synthesis for PbSe nanocrystals was reported by Primera-Pedrozo *et al.* [36]. Aqueous synthesis provides QDs which are ready for use as biological fluorescent agents. The challenge with this synthetic technique is however the fact that it produces QDs with low quantum yields (QY) [37]. High-temperature coordinating solvents produce QDs with higher crystallinity, better stability and higher fluorescence efficiency as compared to aqueous synthetic protocols [38].

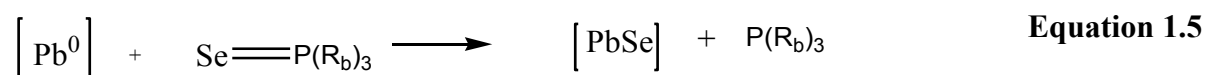
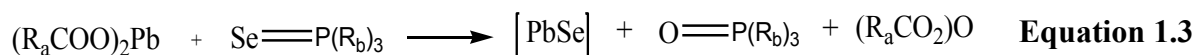
1.3.2 Organometallic synthesis

High-temperature solution-phase synthesis provides a method for preparing uniform nanocrystals for a variety of metals and semiconductors. These methods result in the formation of nanocrystals consisting of an inorganic core surrounded by an organic monolayer [4]. The synthesis of these nanocrystals generally follows a scheme involving a short nucleation event followed by slower growth on the existing nuclei. The major techniques used in QD synthesis include the hot injection and heating-up techniques.

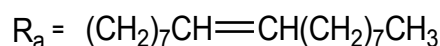
1.3.2.1 Hot injection technique

This technique involves the rapid injection of a precursor solution at room temperature into a hot reaction medium in the presence of carefully chosen surfactant molecules [18]. Generally two procedures are carried out in the hot injection technique; firstly the reaction precursors are pre-mixed in a suitable solvent at a temperature low enough to preclude any reaction. This mixture is then injected into a hot solvent allowing nucleation to take place [39]. The other procedure involves preparing one precursor (commonly metal precursor) at high temperature and maintaining it at the injection temperature then injecting a room temperature solution of the chalcogen precursor [40]. The temperature of the solution is sufficient to decompose the reagents forming a supersaturation of species in solution that is relieved by nucleation of nanocrystals. Upon nucleation, the concentration of the species in solution drops below the critical concentration for nucleation, and further materials can only add to the existing nuclei [4]. The injection of cool reactants into the reaction mixture effectively lowers the reaction temperature allowing the nuclei to grow at lower temperatures than that of the nucleation process. This control of the size and shape of the semiconductor nanocrystals in these QDs is achieved through the separation of the nucleation and growth processes [18]. In this technique the surfactant performs several functions, it acts as a coordinating solvent controlling the QD growth and stabilizing them, it binds to the QD surface hence slowing down the growth kinetics by preventing the addition of monomers to the surface, it also prevents the aggregation of QDs and passivates their surface [18]. Steckel *et al.* studied two possible mechanisms of lead chalcogenide NC formation using ^{31}P NMR to monitor compounds formed during synthesis [41]. They proposed reaction mechanisms based on two possible ionic states of the participating ions. In the first reaction Se^{2-} ions reacted with Pb^{2+} to produce PbSe QDs as shown in **Equation 1.3** below. The proposed reaction mechanism is shown in **Scheme 1.1** [41]. The second method proposes a reaction in which lead oleate is

first reacted with diphenylphosphine (DPP) to reduce Pb^{2+} to Pb^0 which is then reacted with trioctylphosphine selenide (provides Se^0 ions) to form PbSe QDs (**Equation 1.4** and **Equation 1.5**) The proposed reaction mechanism for the DPP mediated reaction is shown in **Scheme 1.2** [41].

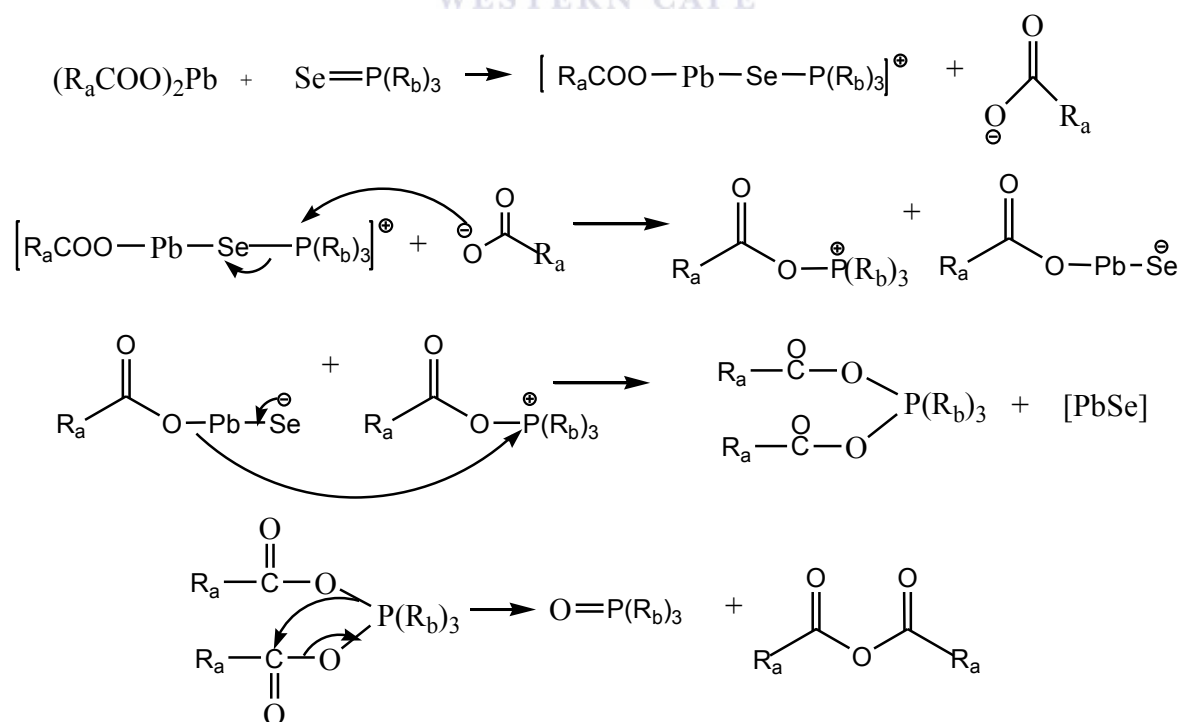


Where

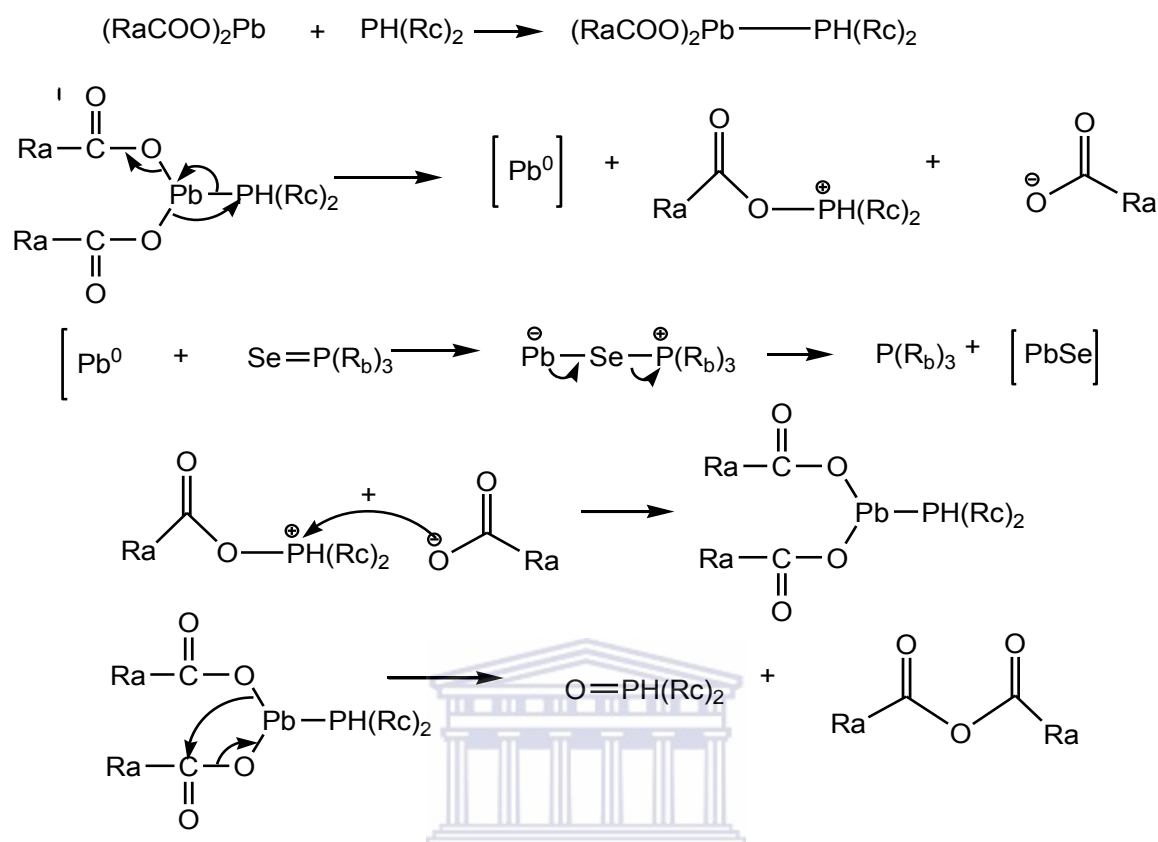


$\text{R}_b = \text{Octyl}$

$\text{R}_c = \text{Phenyl}$



Scheme 1.1 Proposed mechanism for PbSe nanocrystal formation [41]



Scheme 1.2 Proposed mechanism for DPP mediated PbSe nanocrystal formation [41]

1.3.2.2 Heating-up technique

In this technique all the reactants are mixed at a relatively low temperature then the mixture is slowly heated to achieve the required temperature. The requisite supersaturation is achieved by a controlled ramp of the solution temperature which accelerates the chemical reaction. A burst of nucleation relieves the supersaturation as in the hot-injection method. Adjusting the temperature to keep the rate at which the reagents react less than or equal to the rate at which material adds to the existing nuclei ensures that the supersaturated state is never revisited hence inhibiting the formation of new nuclei [4].

The systematic adjustment of the reaction conditions e.g. time, temperature, concentration and chemistry of reagents and surfactants can be used to control QD size and thus prepare a size series of QD samples. In general, QD sizes increase with increasing reaction time, as

more material adds to QD surfaces, and with increasing temperature, as the rate of addition of material to the existing nuclei increases [4].

1.4 Ostwald ripening

Some systems exhibit a second, distinct growth phase known as Ostwald ripening, in which the smaller molecules dissolve and redeposit on the larger QDs to reach a more thermodynamically stable state. Ostwald ripening occurs because molecules on the surface of particles are more energetically unstable than those within [4]. Therefore the unstable surface molecules often go into solution shrinking the particle over time and increasing the number of free molecules in solution. When the solution is saturated with the molecules from the shrinking particles, those free molecules will redeposit on the larger particles (**Figure 1.1**). Thus small particles decrease in size until they disappear and material deposits on the larger particles making them grow even larger. Higher solution temperatures enhance Ostwald ripening, also leading to larger average QD sizes [4].

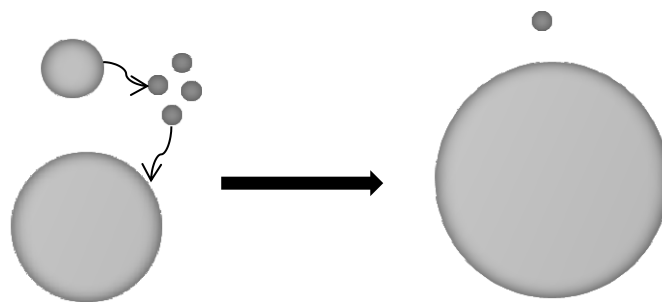


Figure 1.1 Representation of Ostwald ripening

1.5 Surface modification

Colloidal QDs are stabilized with a layer of organic molecules to prevent them from aggregating and to provide them with solution stability [23]. These molecules are often referred to as surfactants, capping agents or ligands [42]. Over the years, various substances have been used as surfactants during QD synthesis. Some of these surfactants can also be used as solvents during the QD synthesis and such solvents are generally known as coordinating solvents. Of these, the most common are trioctylphosphine (TOP) and trioctylphosphine oxide (TOPO). Others including oleylamine (OLA) have also been reported [43]. Surfactant molecules play a major role during nucleation and growth [44]. These molecules are dynamically bonded on the QD surface during nucleation and growth phases. An increase in ligand concentration may therefore lead to restriction of monomer formation hence reduce the number of nuclei formed or restrict monomer addition to nuclei [45,46]. If the restriction of monomer formation is predominant, more monomers will be left in solution after the nucleation stage resulting in the formation of larger QDs. On the other hand, if the restriction of monomer addition to nuclei is predominant, smaller QDs will be formed with increased ligand concentration. These effects have been investigated in group II-VI nanocrystals as well as group IV-VI nanocrystals. In group II-VI systems, an increase in ligand concentration leads to larger QDs being formed as demonstrated in CdSe QDs by Bullen and Mulvaney [45] while in group IV-VI systems, smaller QDs are formed as shown by Dai *et al.* in PbSe QDs [46]. These observations can be attributed to the selective adsorption of the ligand on the surface atoms.

1.5.1 Aqueous solubilization

QDs are mostly produced in nonpolar organic solutions using aliphatic coordinating ligands and as such are only soluble in these nonpolar organic solvents, making phase transfer an

essential and nontrivial step for the QDs to be useful as biological reporters [47]. To render quantum dots biocompatible, their organic passivating agents have to be replaced with hydrophilic groups which will allow them to dissolve in aqueous media. Coating of QDs with hydrophilic reagents greatly improves their applicability in *in vivo* and *in vitro* imaging mainly by improving their compatibility with different biological environments and their chemical stability [47]. QD encapsulation technologies are based on the surface modification of small-molecule ligands, to produce highly water-soluble and bright QDs. The purpose of the surface coating is to improve the stability of the nanocrystals, as well as prevent the leakage of ions from the nanocrystals to the surroundings. This aims at effectively eliminating their cytotoxicity. The surface coating should not only make the nanoparticles water-dispersible, but may also improve their long-term circulation in the body [25]. An ideal water-soluble ligand should meet the following requirements: (1) provide QD stability and solubility in biological buffers; (2) maintain a high resistance to photobleaching and other photophysical properties in aqueous media; (3) have functional groups which are able to conjugate to biomolecules; (4) minimize overall hydrodynamic size [33]. Two general strategies have been developed to render hydrophobic QDs soluble in aqueous solution: ligand exchange and encapsulation by amphiphilic polymers [33,38].

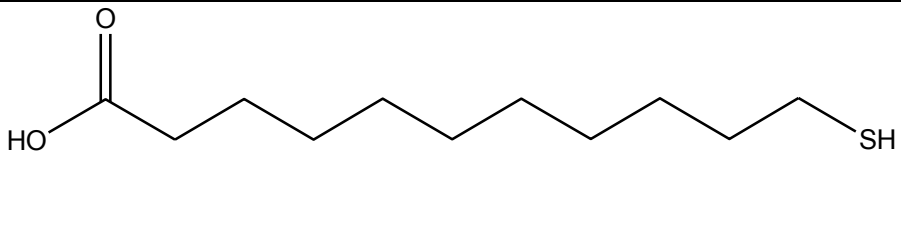
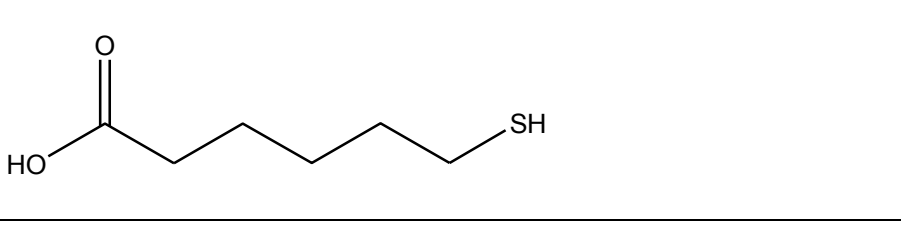


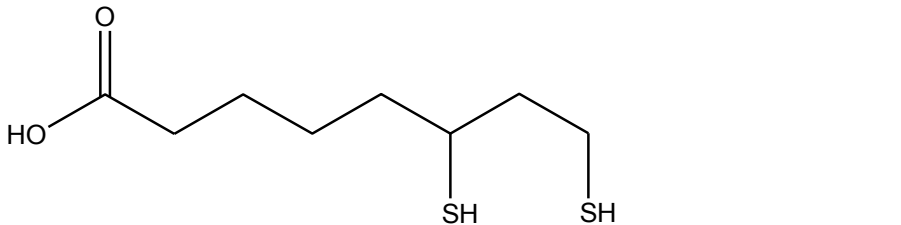
1.5.1.1 Ligand Exchange

This technique involves the displacement of the native hydrophobic ligands from the surface of QDs through mass action and replacing them with heterobifunctional ligands which have one functional group that binds to the QD surface, and another functional group that is hydrophilic. Ligand exchange is carried out in a biphasic system with the QDs being transferred from the organic phase into the aqueous phase [48]. Generally, the as-synthesized QDs are dissolved in an organic solvent (commonly chloroform due its high density) then an aqueous solution of the hydrophilic ligand is added to the QD solution [49]. This mixture is

shaken to allow the QDs to interact with the ligands present in the aqueous phase. The hydrophobic ligands are displaced from the QD through mass action, as the new bifunctional ligand adsorbs to render water solubility [33]. Centrifugation allows the phase separation to be restored and the QDs with the hydrophilic ligands are now suspended in the aqueous phase. Sometimes reflux is necessary to promote desorption of organic ligands from the QD surface. Where reflux is carried out, the temperature is carefully maintained lower than the growth temperature to avoid Ostwald ripening [50].

Using this method, (CdSe)ZnS QDs have been coated with mercaptoacetic acid and (3-mercaptopropyl) trimethoxysilane, both of which contain basic thiol groups which bind to the QD surface atoms, yielding QDs displaying carboxylic acids or silane monomers, respectively. 11-Mercaptoundecanoic acid (MUA), 16-mercaptohexadecanoic acid (MHDA), and aminoethanethiol (AET)-capped PbSe QDs have been successfully prepared following the exchange of surface oleic acid molecules with MUA, MHDA and AET respectively. The ligand exchanged QDs showed red shifted emissions as compared to their organic counterparts but with reduced emission intensities. Similar results were obtained for PbS QDs with MUA, MHDA and AET ligands [49]. The most common types of ligands used in ligand exchange are mercaptocarboxylic acids some of which are shown in **Table 1.1** below. Mercaptocarboxylic acids bind to the QD surface using a thiol linker while utilizing the carboxylate ion to provide hydrophilicity (**Figure 1.2**).

Table 1.1 Some Mercaptocarboxylic acids used in ligand exchange reactions

 <chem>CCCCCCCCCCCC(=O)O</chem>	11-Mercaptoundecanoic acid (MUA)
 <chem>CCCCCC(=O)O</chem>	6-Mercaptohexanoic acid (MHA)
 <chem>CCC(=O)O</chem>	3-Mercaptopropionic acid (MPA)
 <chem>CC(=O)O</chem>	2-Mercaptoacetic acid (MAA) or Thioglycolic acid (TGA)
 <chem>CCCC(CS)CS</chem>	Dihydrolipoic acid (DHLA)

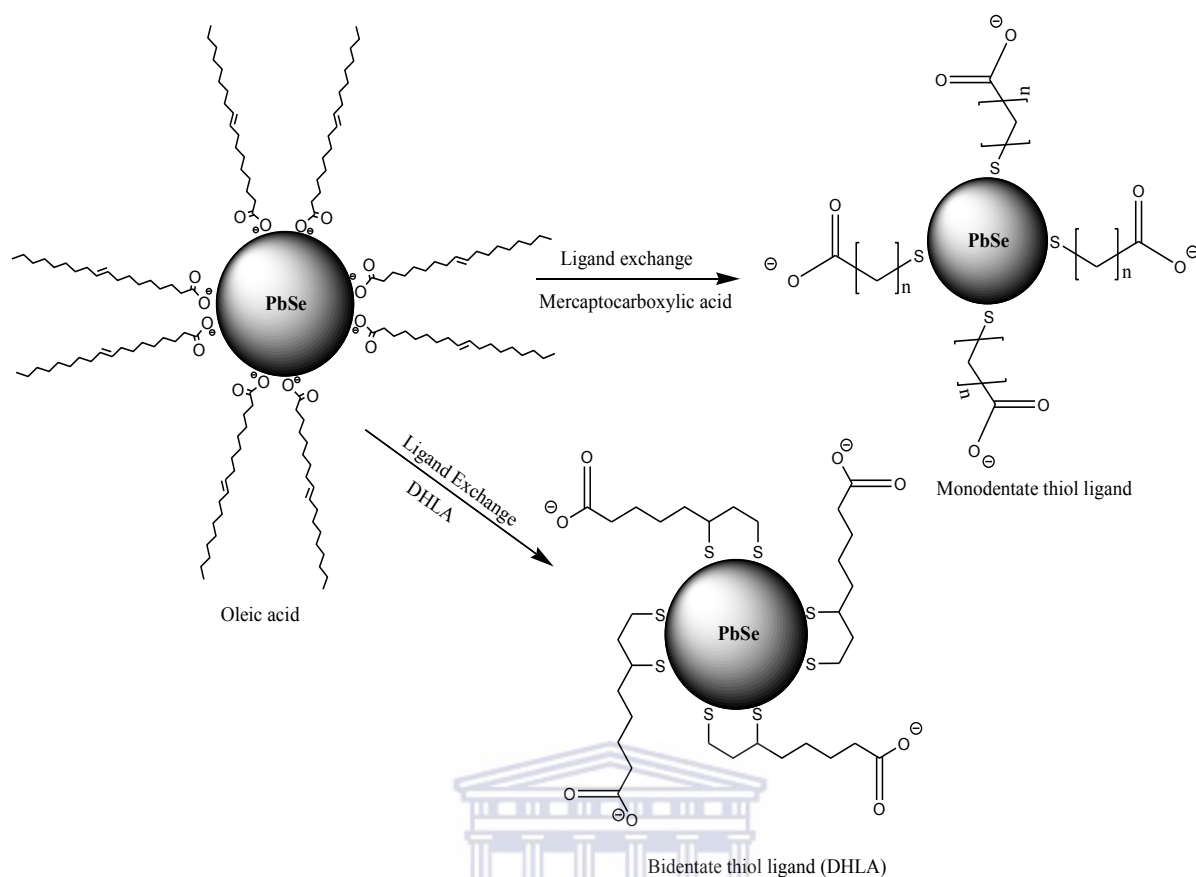


Figure 1.2 Ligand exchange of oleic acid capped PbSe QDs with monodentate and bidentate thiol ligands

UNIVERSITY of the
WESTERN CAPE

The stability of these mercaptocarboxylic acids on PbSe QD surfaces have been investigated and it can be concluded that the longer the chain length the more photostable the QD and the better its solution stability [42]. In aqueous synthesis of PbSe QDs however, shorter chain mercaptocarboxylic acids were found to be more favourable owing to their higher solubility in water and lower stabilization energies of the Pb-ligand bond [36].

Although ligand exchange is fairly simple, straight forward and generates QDs that are useful for biological assays, it is commonly associated with decreased fluorescence efficiency evident by significant loss of the QDs photoluminescence properties and a propensity to aggregate and precipitate in biological buffers [37,38].

1.5.1.2 Amphiphilic polymer encapsulation

More recently, it has been shown that some of the problems mentioned above can be alleviated by retaining the native coordinating ligands on the surface, and instead covering the hydrophobic QDs with amphiphilic polymers. This encapsulation method yields QDs that can be dispersed in aqueous solution and remain stable for long periods of time due to a protective hydrophobic bilayer surrounding each QD through hydrophobic interactions. Silica and polyethylene glycol (PEG) phospholipid dual layer was successfully used to coat PbS QDs as reported by Wang *et al.* [25]. The dual layer was able to transfer the QDs to aqueous phase and chemically stabilize the PbS QDs. This layer completely passivates the QD surface preventing the leakage of heavy metal ions [25].

Table 1.2 shows some of the currently used QD aqueous solubilization strategies and their mechanisms of interaction. It is however of utmost importance that after the transfer into aqueous media the excess ligands or amphiphiles are eliminated from the QD solution by way of purification. The QD properties should also be considered when choosing a solubilization method. As noted in ligand exchange above, the fluorescence properties may be compromised when using this solubilization method. Generally the overall QD size will depend on the coating thickness. While coating with amphiphilic polymers is likely to retain most of the QD properties, it is likely to result in large particles which may preclude their uptake into cells via endocytosis or disrupt signal transduction in sensing applications that utilize distance dependent fluorescence resonance energy transfer (FRET) [33].

Table 1.2 Representation of QD aqueous solubilization and biofunctionalization strategies. Ligands provide linkage to QD (pink), water solubility (blue) and a biomolecule linking functionality. Reprinted with permission from [48], Copyright 2005, Macmillan Publishers Ltd.

QDs as synthesized ^{5,24,27}		Soluble in: toluene hexanes chloroform	Soluble in: basic buffer	
Biofunctionalization 		QD-Cap linking functionality 		
Cap-biomolecule linking functionality 		Water solubility 		
Representative surface-capping strategies		Mechanism of interaction		Examples
a	Monothiolated caps $n = 1$: mercaptoacetic acid $n = 2, 10, 15$: benzyl Hydrophillic $HS(CH_2)_{11}(OCH_2CH_2)_4OR$ R = -H, -CH ₂ COOH	 Dative thiol bond		Mercaptopropionic acids ^{4,39} Alkylthiol terminated DNA ⁴¹ Thioalkylated oligo-ethyleneglycols ³²
b	Bidentate thiols $R = -OH$ $-(OCH_2CH_2)_nOH$ $n = 3, 5, \sim 12$	 Two interactions/ligand		Dihydrolipoic acid derivatives ^{26,43}
c	Silane shell or box dendrimer $R = -SH, -NH_2, -PO_2CH_3$	Hydrophobic Hydrophillic	 Crosslinked shell	Mercaptopropyl silanols ^{3,40} Amine box dendrimers ³¹
d	Hydrophobic interactions $R = \text{Streptavidin}$	Hydrophobic Hydrophillic	 TOP/TOPO	Phosphatidylethanol amine Phosphatidylcholine micelles ³³ Modified acrylic acid polymer ^{33,44,45} Poly(maleic anhydride) alt-1-tetradecene ⁶⁵
e	Functionalized oligomeric phosphines $R = \text{NH}_2, \text{COX}$ X = OH: NH-Streptavidin Hydrophillic	Hydrophobic Hydrophillic		Oligomeric phosphines ³⁷
f	Amphiphilic triblock copolymer Hydrophillic Hydrophobic	Hydrophobic Hydrophillic	 TOP/TOPO *Site for EDC-based antibody conjugation	Amphiphilic triblock copolymer ⁴⁶
g	Amphiphilic saccharides $R = -(CH_2)_{10}CH_3$ X = -O(CH ₂) ₂ -	Hydrophobic Hydrophillic	 Internal alkanes interdigitate with TOPO	Amphiphilic saccharides ³⁶
h	Direct attachment of protein/peptides to QD surface Metal-affinity coordination Maltose binding protein-(H) ₅ -COOH Biotin-G-Cys-E-Cys-G-G-Cys-E-Cys-G-Cha-C-C-Cha-Cmd	Dative thiol bonding Cys = cysteine Cmd = carboxamide Cha = 3-cyclohexylalanine		Phytochelatin- α -peptides ¹⁹ Histidine-rich epitopes ⁵⁰ Polyhistidine metal-affinity coordination ⁵¹⁻⁵⁴

1.6 Application of QDs in diagnostic studies

Fluorescence is the most common method of detecting and quantitating biomolecules [51]. As a result of this, photons have been used as a source of information for the diagnosis and treatment of numerous ailments. Photon detection provides a rapid and cheap way for diagnosis [47,51]. Fluorescent dyes and protein-based fluorophores have been used in several applications over the years including immunoassays, nucleic acid detection, cellular labeling and many others [51]. These fluorophores have however had several challenges which have to be overcome in order to optimize their efficiency. The challenges arise from their photophysical properties which limit their applicability in long-term imaging and multiplexing. The properties include their narrow absorption and broad emission profiles coupled with low photobleaching thresholds [48]. Some of these challenges can be addressed with the use of quantum dot fluorophores which have broad absorption and narrow symmetrical emission profiles, high resistance to photobleaching, photo degradation and chemical degradation. CdSe/ZnS QDs have offered numerous possibilities as fluorophores owing to their chemistry which has been widely studied [48]. They offer tunable emissions within the visible region by varying the QD size. **Figure 1.3** summarizes some of the areas of biological interest on the electromagnetic spectrum as well as the emission wavelengths of some QDs.

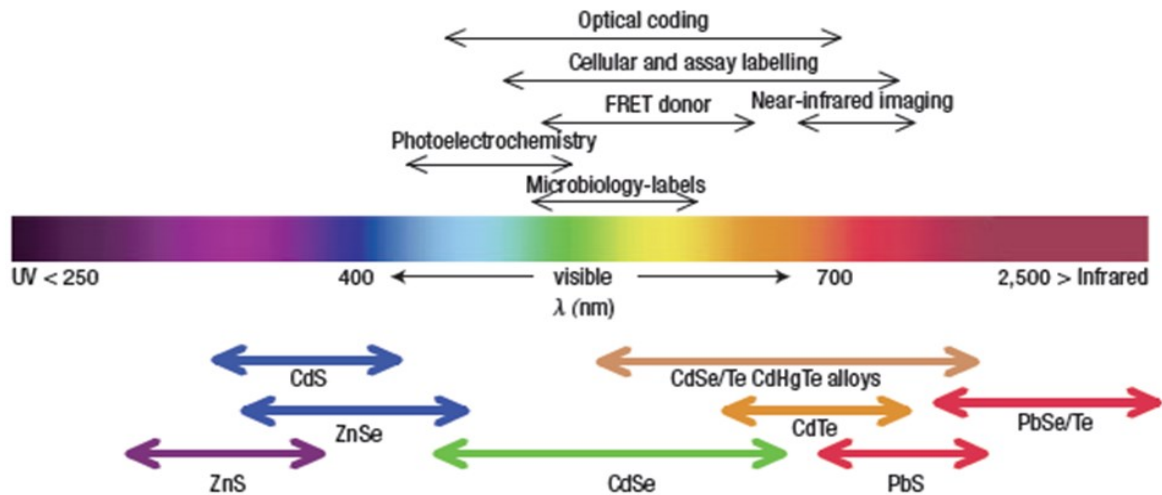


Figure 1.3 Some QD materials and their emission wavelengths on the spectrum. Some of the areas of biological interest are also shown. Reprinted with permission from [48], Copyright 2005, Macmillan Publishers Ltd.

1.6.1 Near-infrared (NIR) QDs

NIR fluorescence techniques enable the *in vivo* imaging of physiological, metabolic and molecular functions. This is made possible by the diagnostic window (NIR window) which can be explored for sensitive detection techniques [20]. QDs can be used as biological contrast agents for optical imaging particularly for deep tissue imaging [20]. Diseases like cancer and some disorders associated with the immune system require specialized diagnostic techniques due to the molecular changes in the tissue which are very complex. Early diagnosis is a key way to help in the management and possibly treatment of these diseases. Since these diseases especially cancers heavily spread through molecular changes, their diagnostic methods have majorly been based on the manifestation of the molecular changes that underlie the disease. It is however possible to detect or diagnose the disease early by monitoring the biomarkers that are disease-specific [20]. This allows disease diagnosis to be carried out at an early stage of the disease which makes early treatment possible. The current imaging methods focus on tumor monitoring which in most cases the tumor is already enlarged and may require very expensive procedures to remove. Imaging and monitoring of

molecular changes that underlie the disease can allow for early detection of diseases. Biological imaging is however complex due to the presence of biological media which also absorb and emit light similar to the fluorescent probes commonly used. This poses a challenge which may lead to inaccurate results. PbSe QDs absorb light over a wide range from ultra-violet (UV) through near-infrared (NIR). They emit light in the NIR region where tissue auto fluorescence is minimal making them useful tools for fluorescence imaging.



1.7 Problem statement

Group II-VI nanocrystals have found applications in various biological systems due to their fluorescence within the first biological window of wavelengths between 650 nm and 950 nm. Though they have been used for optical imaging of live animals, this optical window does not give optimal results due to tissue autofluorescence which produces substantial background noise and the tissue penetration depth is limited to between 1 and 2 cm [27]. Studies have suggested that it would be possible to improve signal to noise ratios by use of nanocrystals that emit at light within the second biological window of wavelengths between 1000 nm and 1350 nm. This biological window, which is also considered to be highly sensitive for *in vivo* imaging, has however not been fully explored due to lack of biocompatible fluorescent probes [27]. Single walled carbon nanotubes (SWCNT) that emit between 950 nm and 1400 nm have been used to map blood vessels with minimal background autofluorescence [52]. The structure of the nanotubes has however elicited some concerns due to tissue damage and cytotoxicity being observed in lungs following inhalation.

Semiconductor QDs in general are more promising than nanotubes because their size and shape can be finely adjusted to produce the desired properties due to their tunability [27]. Lead chalcogenides in particular offer emissions of wavelengths above 1000 nm which are well within the second biological window thus can be more favourable for deep tissue imaging than the currently used II-VI nanocrystals. They also have very large Bohr radii as compared to cadmium systems [7,47,53,54]. With a larger excitonic Bohr radius, smaller nanocrystal sizes will be required as compared to the currently used systems. In this study the synthesis and characterization of NIR emitting PbSe QDs was investigated. The reaction conditions were also varied in order to investigate the effects these would have on the QD properties. Aqueous and organometallic synthetic protocols were employed in order to determine the route that provided the most stable QDs. The cytotoxicity of some of the

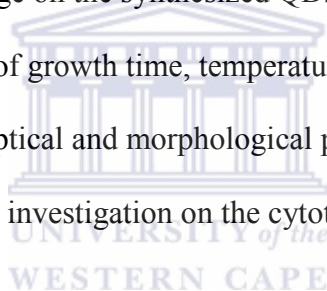
synthesized QDs was investigated in order to determine whether the QDs can indeed be used in diagnostic studies without toxic effects on cells.

1.8 Aims and objectives

The aim of this study is to synthesize and characterize PbSe quantum dots and to investigate their applicability in diagnostic studies.

The specific objectives are as follows:

- a) To synthesize PbSe quantum dots via the organometallic and aqueous routes
- b) To characterize the quantum dots using photoluminescence (PL) spectroscopy, transmission electron microscopy (TEM) and X-ray Diffraction (XRD)
- c) To perform ligand exchange on the synthesized QDs
- d) To investigate the effects of growth time, temperature, ligand purity, lead and selenium sources on the optical and morphological properties of PbSe QDs
- e) To carry out a preliminary investigation on the cytotoxicity of the synthesized QDs



1.9 References

- [1] Joo J, Pietryga JM, McGuire JA, Jeon S, Williams DJ, Wang H, Klimov VI. A reduction pathway in the synthesis of PbSe nanocrystal quantum dots. *J. Am. Chem. Soc.*, **2009**, 131, 10620-10628.
- [2] “Nanotechnology”. Oxford Dictionaries. Oxford University Press. <http://www.oxforddictionaries.com/definition/english/nanotechnology> (accessed November 10, 2013).
- [3] Burger JR. Human memory modeled with standard analog and digital circuits: inspiration for man-made computers. *United States of America; John Wiley & Sons, Inc.* **2009**, p. 34. (E-book accessed 11 November 2013).
- [4] Murray CB, Sun S, Gaschler W, Doyle H, Betley TA, Kagan CR. Colloidal synthesis of nanocrystals and nanocrystal superlattices. *IBM J. Res. Dev.*, **2001**, 45, 47-56.
- [5] Amiot CL, Xu S, Liang S, Pan L, Zhao JX. Near-Infrared Fluorescent Materials for Sensing of Biological Targets. *Sensors*, **2008**, 8, 3082-3105.
- [6] Reiss P, Protière M, Li L. Core/shell semiconductor nanocrystals. *Small*, **2009**, 5, 154-168.
- [7] Wise FW. Lead salt quantum dots: the limit of strong quantum confinement. *Acc. Chem. Res.*, **2000**, 33, 773-780.
- [8] Harbold JM. The electronic and optical properties of colloidal lead-selenide semiconductor nanocrystals. *PhD Thesis*, Cornell University **2005**.
- [9] Smith AM, Dave S, Nie S, True L, Gao X. Multicolor quantum dots for molecular diagnostics of cancer. *Expert Rev. Mol. Diagn.*, **2006**, 6, 231-244.
- [10] Dabbousi BO, Rodriguez-Viejo J, Mikulec FV, Heine JR, Mattoussi H, Ober R, Jensen KF, Bawendi MG. (CdSe)ZnS Core-Shell quantum dots: Synthesis and characterization

-
- of a size series of highly luminescent nanocrystallites. *J. Phys. Chem. B*, **1997**, 101, 9463-9475.
- [11] Brus L. Electronic wave functions in semiconductor clusters: Experiment and theory. *J. Phys. Chem.*, **1986**, 90, 2555-2560.
- [12] Guo L. Synthesis and characterization of II-VI and IV-VI colloidal semiconductor quantum dots. *PhD Thesis*. University of Rochester **2007**.
- [13] Brennan JG, Siegrist T, Carroll PJ, Stuczynski SM, Brus LE, Steigerwald ML. The preparation of large semiconductor clusters via the pyrolysis of a molecular precursor. *J. Am. Chem. Soc.*, **1989**, 111, 4141-4143.
- [14] Zhao Y. Resonance fluorescence and electron spin in semiconductor quantum dots *Doctoral thesis*. University of Heidelberg **2009**.
- [15] Peterson JJ, Krauss TD. Fluorescence spectroscopy of single lead sulfide quantum dots. *Nano Lett.*, **2006**, 6, 510-514.
- [16] Lipovskii A, Kolobkova E, Petrikov V, Kang I, Olkhovets A, Krauss T, Thomas M, Silcox J, Wise F, Shen Q, Kycia S. Synthesis and characterization of PbSe quantum dots in phosphate glass. *Appl. Phys. Lett.*, **1997**, 71, 3406-3408.
- [17] Yu WW, Falkner JC, Shih BS, Colvin VL. Preparation and characterization of monodisperse PbSe semiconductor nanocrystals in a noncoordinating solvent. *Chem. Mater.*, **2004**, 16, 3318-3322
- [18] Mushonga P, Onani MO, Madiehe AM, Meyer M. Indium phosphide-based semiconductor nanocrystals and their applications. *J. Nanomater.*, **2012**, 2012, 869284.
- [19] van Veggel FCJM. Near-infrared quantum dots and their delicate synthesis, challenging characterization, and exciting potential applications. *Chem. Mater.*, <http://pubs.acs.org/doi/abs/10.1021/cm4021436> (accessed September 25, 2013).

-
- [20] Aswathy RG, Yoshida Y, Maekawa T, Kumar DS. Near-infrared quantum dots for deep tissue imaging. *Anal. Bioanal. Chem.*, **2010**, 397, 1417–1435.
- [21] Jin S, Hu Y, Gu Z, Liu L, Wu H. Application of quantum dots in biological imaging. *J. Nanomater.*, **2011**, 2011, 834139.
- [22] Geyter BD, Justo Y, Moreels I, Lambert K, Smet PF, Thourhout DV, Houtepen AJ, Grodzinska D, Donega CM, Hens Z. The different nature of band edge absorption and emission in colloidal PbSe/CdSe core/shell quantum dots. *ACS Nano.*, **2011**, 5, 58-65.
- [23] Mushonga P. Fabrication of type-I indium-based near-infrared emitting quantum dots for biological imaging applications. *PhD Thesis*, University of the Western Cape **2013**. (Unpublished results).
- [24] Ornberg RL, Harper TF, Liu H. Western blot analysis with quantum dot fluorescence technology: a sensitive and quantitative method for multiplexed proteomics. *Nat. Methods*, **2005**, 2, 79-81.
- [25] Wang D, Qian J, Cai F, He S, Han S, Mu Y. Green'-synthesized near-infrared PbS quantum dots with silica-PEG dual-layer coating: ultrastable and biocompatible optical probes for in vivo animal imaging. *Nanotechnology*, **2012**, 23, 245701 (9pp).
- [26] Bencherif Y, Boukra A, Zaoui A, Ferhat M. Lattice dynamics of lead chalcogenides. *Infrared Phys. Techn.*, **2011**, 54, 39-43.
- [27] Smith AM, Mancini MC, Nie S. Second window for in vivo imaging. *Nat. Nanotechnol.*, **2009**, 4, 710–711.
- [28] Bakueva L, Musikhin S, Hines MA, Chang TWF, Tzolov M, Scholes GD, Sargent EH. Size-tunable infrared (1000-1600 nm) electroluminescence from PbS quantum-dot nanocrystals in a semiconducting polymer. *Appl. Phys. Lett.*, **2003**, 82, 2895-2897.

-
- [29] Borelli NF, Smith DW. Quantum confinement of PbS microcrystals in glass. *J. Non-Cryst. Solids*, **1994**, 180, 25-31.
- [30] Murray CB, Norris DJ, Bawendi MG. Synthesis and characterization of nearly monodisperse CdE (E = S, Se, Te) semiconductor nanocrystallites. *J. Am. Chem. Soc.*, **1993**, 115, 8706-8715.
- [31] Sowers KL, Swartz B, Krauss TD. Chemical mechanisms of semiconductor nanocrystals synthesis. *Chem. Mater.*, **2013**, 25, 1351-1362.
- [32] Reiss P, Protière M, Li L. Core/shell semiconductor nanocrystals. *Small*, **2009**, 5, 154-168.
- [33] Zhang Y, Clapp A. Overview of stabilizing ligands for biocompatible quantum dot nanocrystals. *Sensors*, **2011**, 11, 11036-11055.
- [34] Gaponik N, Talapin DV, Rogach AL, Hoppe K, Shevchenko EV, Kornowski A, Eychmüller A, Weller H. Thiol-capping of CdTe nanocrystals: An alternative to organometallic synthetic routes. *J. Phys. Chem. B*, **2002**, 106, 7177-7185.
- [35] Yu Y, Zhang K, Li Z, Sun S. Synthesis and luminescence characteristics of DHLA-capped PbSe quantum dots with biocompatibility. *Opt. Mater.*, **2012**, 34, 793–798.
- [36] Primera-Pedrozo OM, Arslan Z, Rasulev B, Leszczynski J. Room temperature synthesis of PbSe quantum dots in aqueous solution: stabilization by interactions with ligands. *Nanoscale*, **2012**, 4, 1312-1320.
- [37] Zhelev Z, Bakalova R, Ohba H, Jose R, Imai Y, Baba Y. Uncoated, broad fluorescent, and size-homogeneous CdSe quantum dots for bioanalyses. *Anal. Chem.*, **2006**, 78, 321-330.
- [38] Smith AM, Duan H, Mohs AM, Nie S. Bioconjugated quantum dots for *in vivo* molecular and cellular Imaging. *Adv. Drug Deliv. Rev.*, **2008**, 60, 1226–1240.

-
- [39] Du H, Chen C, Krishnan R, Krauss TD, Harbold JM, Wise FW, Thomas MG, Silcox J. Optical properties of colloidal PbSe nanocrystals. *Nano Lett.*, **2002**, 2, 1321-1324.
- [40] Stouwdam JW, Shan J, van Veggel FCJM, Pattantyus-Abraham AG, Young JF, Raudsepp M. Photostability of colloidal PbSe and PbSe/PbS core/shell nanocrystals in solution and in the solid state. *J. Phys. Chem. C*, **2007**, 111, 1086-1092.
- [41] Steckel JS, Yen BKH, Oertel DC, Bawendi MG. On the mechanism of lead chalcogenide nanocrystal formation. *J. Am. Chem. Soc.*, **2006**, 128, 13032-13033.
- [42] Aldana J, Wang A, Peng X. Photochemical instability of CdSe nanocrystals coated by hydrophilic thiols. *J. Am. Chem. Soc.*, **2001**, 123, 8844-8850.
- [43] Pan Y, Bai H, Pan L, Li Y, Tamargo MC, Sohel M, Lombardi JR. Size controlled synthesis of monodisperse PbTe quantum dots: using oleylamine as the capping ligand. *J. Mater. Chem.*, **2012**, 22, 23593-23601.
- [44] Yu WW, Peng X. Formation of high-quality CdS and other II-VI semiconductor nanocrystals in noncoordinating solvents: tunable reactivity of monomers. *Angew. Chem. Int. Ed.*, **2002**, 41, 2368-2371.
- [45] Bullen CR, Mulvaney P. Nucleation and growth kinetics of CdSe nanocrystals in octadecene. *Nano Lett.*, **2004**, 4, 2303-2307.
- [46] Dai Q, Zhang Y, Wang Y, Wang Y, Zou B, Yu WW, Hu MZ. Ligand effects on synthesis and post-synthetic stability of PbSe nanocrystals. *J. Phys. Chem. C*, **2010**, 114, 16160-16167.
- [47] Cassette E, Helle M, Bezdetsnaya L, Marchal F, Dubertret B, Pons T. Design of new quantum dot materials for deep tissue infrared imaging. *Adv. Drug Deliv. Rev.*, **2013**, 65, 719-731.

-
- [48] Medintz IL, Uyeda HT, Goldman ER, Mattoussi H. Quantum dot bioconjugates for imaging, labelling and sensing. *Nat. Mater.*, **2005**, 4, 435-446.
- [49] Hyun B, Chen H, Rey DA, Wise FW, Batt CA. Near-Infrared fluorescence imaging with water-soluble lead salt quantum dots. *J. Phys. Chem. B*, **2007**, 111, 5726-5730.
- [50] Li L, Daou TJ, Texier I, Chi TTK, Liem NQ, Reiss P. Highly luminescent CuInS₂/ZnS core/shell nanocrystals: cadmium-free quantum dots for *in vivo* imaging. *Chem. Mater.*, **2009**, 21, 2422–2429.
- [51] Sapsford KE, Pons T, Medintz IL, Mattoussi H. Biosensing with luminescent semiconductor quantum dots. *Sensors*, **2006**, 6, 925-953.
- [52] Welsher K, Liu Z, Sherlock SP, Robinson JT, Chen Z, Daranciang D, Dai H. A route to brightly fluorescent carbon nanotubes for near-infrared imaging in mice. *Nat. Nanotechnol.*, **2009**, 4, 773–780.
- [53] Abdulla MM, Hasan NH, Mohammed HI, Mohamed GH, Al-Hamdani KA, Abdulameer AF. Investigation of optical properties of the PbS/CdS thin films by thermal evaporation. *J. Electron Dev.*, **2012**, 12, 761-766.
- [54] Duan J, Song L, Zhan J. One-pot synthesis of highly luminescent CdTe quantum dots by microwave irradiation reduction and their Hg²⁺-sensitive properties. *Nano Res.*, **2009**, 2, 61-68.

2 Experimental

Various synthetic techniques and materials were used in the synthesis and characterization of PbSe quantum dots for this work. Previously reported procedures were used with some modifications in order to investigate the desired properties.

2.1 Materials

All the experiments were carried out using analytical grade chemicals which were used without further purification. Lead (II) acetate trihydrate ($\text{Pb}(\text{Ac})_2 \cdot 3\text{H}_2\text{O}$), lead (II) oxide (PbO , 99.99 %), selenium powder (100 mesh, 99+ %), 3-Mercaptopropionic acid (MPA, ≥ 99 %), 11-Mercaptoundecanoic acid (MUA, 95 %), trioctylphosphine (TOP, 90 %), tributylphosphine (TBP, 97 %), oleic acid (OA, 90 %), oleic acid (OA, 99 %), 1-octadecene (ODE, 90 %), sodium borohydride powder (NaBH_4 , 98 %), diphenyl ether, oleylamine (OLA), hexane, acetone, chloroform, NaOH pellets, 2-propanol, hydrochloric acid (HCl), nitric acid (HNO_3) were purchased from Sigma Aldrich.

2.2 Instrumentation

Characterization of the synthesized quantum dots (QDs) was carried out using various spectroscopic techniques. These techniques include photoluminescence spectroscopy (PL), X-ray diffraction (XRD), transmission electron microscopy (TEM) energy-dispersive X-ray spectroscopy (EDS) and selected area electron diffraction (SAED).

2.2.1 Photoluminescence spectroscopy (PL)

Some of the qualities that make quantum dots (QDs) very attractive are their superior fluorescence properties. Fluorescence can be defined as the emission of light by a substance

after it has absorbed light or some form of electromagnetic radiation. It can also be defined as the visible or invisible radiation produced from certain substances as a result of incident radiation of short wavelengths such as X-rays or ultraviolet light or the property of absorbing light of short wavelengths and emitting light of longer wavelengths [1]. Spectroscopy on the other hand refers to the quantification of this emitted light. The emission spectra of the synthesized QDs were recorded using a HORIBA NanoLog FL3-22-TRIAX using a liquid nitrogen (N₂) cooled InGaAs near-infrared (NIR) detector. **Figure 2.1** represents the various parts of a HORIBA NanoLog instrument.

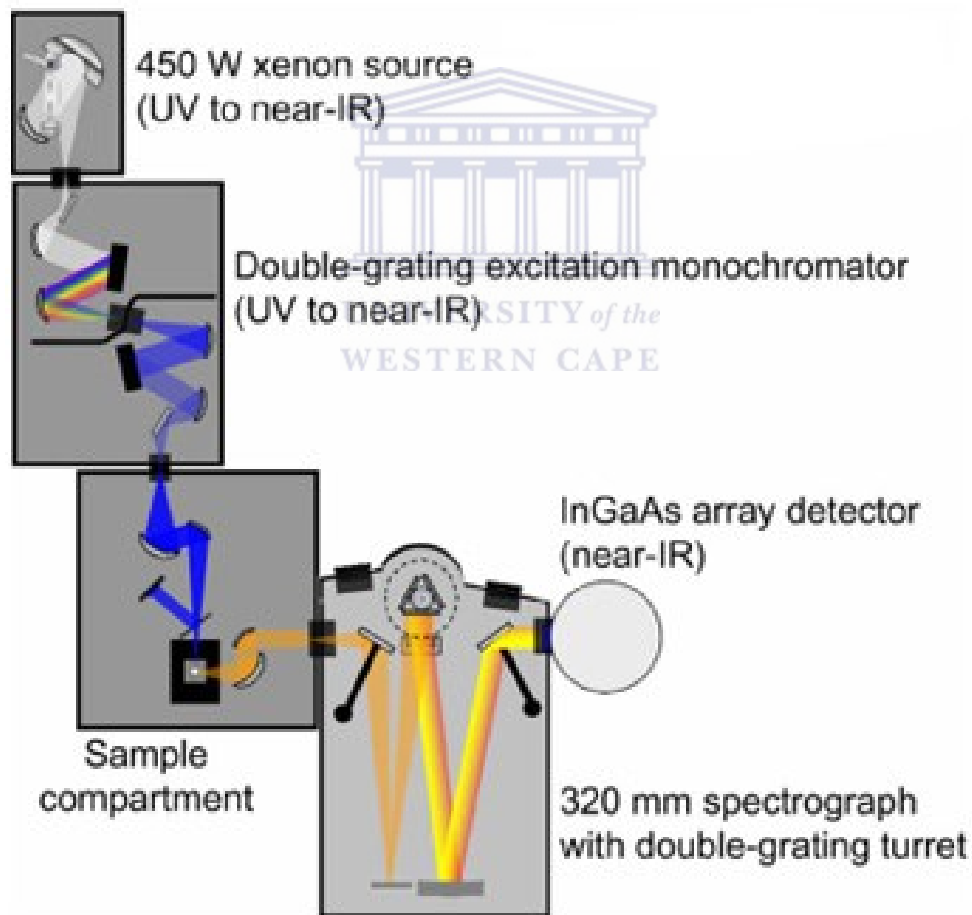


Figure 2.1 Schematic representation of a Horiba Jobinyvon NanoLog, showing the optical path from source through sample to detectors [2]

2.2.2 X-ray diffraction (XRD)

XRD was used to determine the crystal structure of the synthesized nanocrystals. XRD analysis was carried out at iThemba Labs, Cape Town on a Bruker AXS D8 Advanced Diffractometer equipped with a CuK α ($\lambda = 1.5418 \text{ \AA}$) X-ray source. The diffraction patterns obtained were also used to confirm particle sizes obtained from TEM micrographs. These particle sizes were calculated using the scherrer equation (**Equation 2.1**) [3,4].

$$d = \frac{k \lambda}{\beta \cos \theta} \quad \text{Equation 2.1}$$

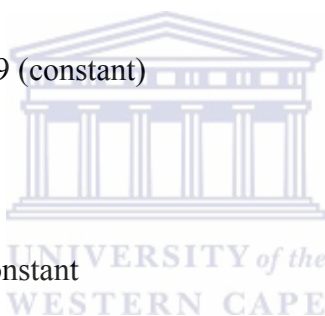
Where

k = shape factor approximately 0.9 (constant)

λ = X-ray wavelength (1.5405 \AA)

β = optical frequency dielectric constant

θ = diffraction angle



2.2.3 Transmission electron microscopy (TEM)

Transmission electron microscopy was used to determine the size and shape of the synthesized QDs. Energy-dispersive X-ray spectroscopy (EDS) was used as a chemical analysis system to quantify the chemical composition of the QDs. EDS relies on the counting of X-rays emitted from the beam-illuminated specimen region as a function of the photon energy [5]. HR-TEM and EDS characterization were carried out on a TECNAI F30ST transmission electron microscope (**Figure 2.2**). Samples for TEM analysis were dispersed in hexane and dropped on carbon film-coated copper grids to form an ultrathin layer which was

dried under an electric bulb for 10 min. Nanocrystal sizes were determined from the TEM micrographs with the aid of ImageJ software.



Figure 2.2 Tecnai™ Transmission electron microscope [6]

2.3 Synthesis and purification of PbSe QDs

PbSe QDs were synthesized through the two major synthetic methods as described in section 1.3 i.e. organometallic and aqueous syntheses. The organometallic synthetic procedure employed was the hot-injection technique.

2.3.1 Organometallic reactions

PbSe QDs were prepared according to a previously reported procedure with some modifications [7]. The reaction was carried out using standard air-free procedures using a glove box and Schlenk line.

2.3.1.1 Preparation of reaction precursors

The lead and chalcogen precursor were prepared separately in three-neck and two-neck round bottom flasks respectively.

2.3.1.1.1 Preparation of Lead precursor

Lead oleate was prepared by drying PbO (223 mg (1mmol)) (or Pb(Ac)₂·3H₂O) under vacuum at 130 °C for 15 min, followed by the addition of 20 mL of octadecene (ODE) and 635 μL (2 mmol) of oleic acid (OA). The mixture was heated under vacuum for 15 min at 130°C till the yellow colour disappeared forming Pb-(oleate)₂ [7,8]. The heating also served to remove excess H₂O and acetic acid. This was followed by bubbling argon gas through the solution for 1 h.

2.3.1.1.2 Preparation of chalcogen precursor

In a 2-neck flask, 158 mg (2 mmol) of elemental selenium was dissolved in 5 mL of TOP or TBP in the glove box. The mixture was stirred at room temperature till all the selenium had dissolved.

2.3.1.2 Preparation of PbSe QDs

Oleic acid-capped PbSe QDs were prepared by maintaining the temperature of the Pb-oleate solution at the required injection temperature and rapidly injecting 2.5 mL (1 mmol equivalent of Se) of TOPSe or TBPS_e solution into the Pb-oleate solution. The QDs were

allowed to grow for 30 min with samples being taken at various intervals for optical characterization.

2.3.1.3 Purification of QDs

The QD solution was purified by adding 20 mL hexane to dissolve the formed QDs. The solution was transferred into 2 mL eppendorf tubes and centrifuged at 6000 revolutions per minute (rpm) for 10 min and unreacted material settled at the bottom of the tubes while QDs remained in the supernatant. The unreacted material was discarded and excess acetone was added to the supernatant till QDs precipitated forming a cloudy solution. This solution was centrifuged at 6000 rpm for 10 min to allow QDs to settle at the bottom with a clear supernatant solution. The supernatant was discarded and the QD pellet was dried and stored in the dark at 4 °C.

2.3.1.4 Ligand Exchange

The synthesized QDs were transferred from organic media to aqueous media by exchanging their hydrophobic surface ligands with hydrophilic ligands.

2.3.1.4.1 3-Mercaptopropionic acid (MPA) ligands

The MPA solution was prepared by dissolving 3 mL MPA in 7 mL deionized water (30 % MPA solution). The solution pH was adjusted using NaOH to pH 11. QD pellet was dissolved in 0.5 mL chloroform in a 2 mL eppendorf tube and 0.5 mL of MPA solution added to the QD solution. The mixture was shaken on a vortex mixer for 4 h. After 4 h the mixture was spun at 6000 rpm for 10 min to separate the aqueous phase from the organic phase. The ligand exchange was also carried out using 50 % and 100 % MPA solutions.

2.3.1.4.2 11-Mercaptoundecanoic acid (MUA) ligands

Ligand exchange with MUA was carried out according to a procedure reported by Hyun *et al.* with some modifications [9].

MUA solution was prepared by dissolving 7 mg MUA in 1 mL chloroform. QD pellet was dissolved in 0.1 mL chloroform. 0.5 mL MUA solution was added to the QD solution and shaken till the QDs flocculated. 0.4 mL NaOH solution (9 mg/mL) was added to the QD solution and shaken on a vortex mixer for 10 min. The solution was centrifuged at 6000 rpm for 2 min to allow for phase separation. The QDs were transferred from the organic phase into the aqueous phase.

2.3.1.5 Investigation of the effects of reaction parameters on the optical and structural properties of PbSe QDs

Several reactions were carried out while varying the injection temperatures, solvent, lead salt, selenium precursor, and ligand used. The reactions are summarised in Table 2.1, Table 2.2, Table 2.3 and Table 2.4 below. The solvents used were 1-octadecene (ODE), diphenyl ether (Ph₂Et), trioctylphosphine (TOP) and oleylamine (OLA). The lead salts used were lead (II) oxide (PbO) and lead (II) acetate trihydrate (Pb(Ac)₂·3H₂O). Selenium precursors used were trioctylphosphine-selenium (TOPSe) and tributylphosphine selenide (TBPSe). Ligands used were 90 % oleic acid (OA) and 99 % oleic acid (99 % OA).

Table 2.1 Effect of injection temperature and growth time

	Solvent	Ligand	Pb source	Se source	Injection Temp (°C)	Growth time (min)
1.	ODE	OA	PbO	TOPSe	150	10
2.	ODE	OA	PbO	TOPSe	150	20
3.	ODE	OA	PbO	TOPSe	150	30
4.	ODE	OA	PbO	TOPSe	121	10
5.	ODE	OA	PbO	TOPSe	121	20
6.	ODE	OA	PbO	TOPSe	121	30
7.	ODE	OA	PbO	TOPSe	90	10
8.	ODE	OA	PbO	TOPSe	90	20
9.	ODE	OA	PbO	TOPSe	90	30

Table 2.2 Effect of solvent

	Solvent	Ligand	Pb source	Se source	Injection Temp (°C)	Growth time (min)
1.	ODE	OA	PbO	TOPSe	121	10
2.	Ph ₂ Et	OA	PbO	TOPSe	121	10
3.	Ph ₂ Et	OA	PbO	TOPSe	90	30
4.	TOP	OA	PbO	TOPSe	90	30
5.	OLA	OA	PbO	TOPSe	90	30

Table 2.3 Effect of lead and selenium sources

	Solvent	Ligand	Pb source	Se source	Injection Temp (°C)	Growth time (min)
1.	ODE	OA	Pb(Ac) ₂	TOPSe	90	30
2.	Ph ₂ Et	OA	Pb(Ac) ₂	TOPSe	90	30
3.	ODE	OA	PbO	TOPSe	90	30
4.	ODE	OA	PbO	TBPSse	90	30
5.	ODE	OA	Pb(Ac) ₂	TOPSe	90	30
6.	ODE	OA	Pb(Ac) ₂	TBPSse	90	30

Table 2.4 Effect of ligand purity

	Solvent	Ligand	Pb source	Se source	Injection Temp (°C)	Growth time (min)
1.	ODE	90% OA	PbO	TBPSse	90	30
2.	ODE	99% OA	PbO	TBPSse	90	30

2.3.2 Aqueous reactions

These reactions were carried out at room temperature with 3-Mercaptopropionic acid used as a capping agent for the synthesized QDs. PbSe nanocrystals were synthesized according to a previously reported method with some modifications [11].

2.3.2.1 Preparation of Lead precursor

Pb(Ac)₂·3H₂O (0.5 mmol) was dissolved in deionised water (50 mL) in a 3-neck round bottom flask and 3-mercaptopropionic acid (5 mmol) was added into the flask forming a cloudy solution (pH 2.48). 5 M NaOH was added drop wise into the flask until a clear solution was obtained (pH 9.06).

2.3.2.2 Preparation of selenium precursor

Selenium stock solution was prepared by dissolving selenium powder (5 mmol) in concentrated nitric acid (HNO₃) in a test tube. Excess HNO₃ was evaporated and the resulting solution topped up to 10 mL with HCl (10 % v/v). Selenium solution (2.5 mL, 0.5 M) was added into a separate 3-neck flask followed by HCl (2.5 mL, 10 % v/v).

2.3.2.3 Synthesis of MPA-capped PbSe QDs

The two flasks were connected via rubber tubing and the remaining necks sealed off using rubber septa. Nitrogen gas was bubbled through the selenium flask into the lead acetate flask with stirring for 30 min. NaBH₄ solution was prepared by dissolving NaBH₄ (1 g) in NaOH solution (10 mL, 0.1 % m/v). PbSe QDs were prepared by adding NaBH₄ solution (10 mL) drop wise into the selenium flask producing H₂Se gas which reacted with Pb-MPA complex to form dark coloured nanocrystals. The gas was allowed to flow for 20 min after the addition of NaBH₄ to allow all the formed H₂Se gas to be used up in the reaction. Stirring was continued for 1 h after the stopping of gas flow to allow nanocrystals to become stable.

2.3.2.4 Purification of QDs

The nanocrystal solution was centrifuged at 6000 rpm for 10 min to remove any unreacted or excess material. 2-Propanol was added in excess to the nanocrystal solution to precipitate the nanocrystals.

2.4 Cytotoxicity experiments

Cytotoxicity experiments were carried out using Caco-2 cells using the water soluble tetrazolium salt (WST-1) assay. Caco-2 cells were cultured in a T25 cm³ tissue culture flask containing Dulbecco's Modified Eagle Medium (DMEM) growth medium, 10 % foetal bovine serum and 1 % antibiotics and incubated at 37 °C until the cells reached ≥ 70 % confluency. The cell growth was monitored using a Nikon light microscope. The culture medium was then removed and the cells washed with phosphate buffer saline (PBS). Trypsin was added to the cells and incubated for about 5-10 min until most of the cells detached from the flask. The growth medium was added to the cells and centrifuged to separate the cells from the supernatant. The cells were re-suspended in PBS followed by centrifugation to obtain the cell pellet which was re-suspended in the growth medium. This was followed by counting the cells in a Countess® Automated cell counter followed by seeding a cell density of 1×10^5 cells/mL in a 96 well plate at a volume of 100 μ L per well. These cells were incubated at 37 °C for 24 h. After the incubation, the spent media was removed and replaced with fresh media containing various concentrations of PbSe quantum dots and again incubated at 37 °C for 24 h. Then 10 μ L of WST-1 was added in each well and incubated for a further 4 h at the same temperature. After the incubation period, the absorbance readings were taken using a BMG Labtech POLARstar Omega micro plate reader. Absorbance readings were taken at 440 nm and 630 nm. 630 nm was used as the reference wavelength and all the absorbance values at 630 nm were subtracted from the corresponding readings at

440 nm. The cell viability data was presented as a percentage with the untreated cells acting as the control therefore providing absolute values or 100 % viability.



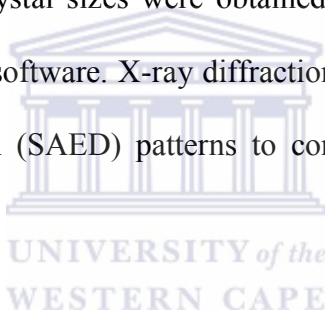
2.5 References

- [1] "fluorescence". Oxford Dictionaries. Oxford University Press. <http://oxforddictionaries.com/definition/english/fluorescence> (accessed September 19, 2013).
- [2] <http://www.lastek.com.au/nir-mainmenu-528/systems-mainmenu-1589/261-horiba-jy-nanolog> (accessed September 19, 2013).
- [3] Li J, Xu J, Zhao L, Xu Q, Fang G. Preparation and characterization of CdSe and PbSe nanoparticles via aqueous solution for nanoparticle-based solar cells. *Mater. Res. Bull.*, **2013**, 48, 1560-1568.
- [4] Yu Y, Zhang K, Li S, Sun S. Synthesis and luminescence characteristics of DHLA-capped PbSe quantum dots with biocompatibility. *Opt. Mater.*, **2012**, 34, 793-798.
- [5] Wang ZL. Transmission electron microscopy of shape-controlled nanocrystals and their assemblies. *J. Phys. Chem. B*, **2000**, 104, 1153-1175.
- [6] <http://www.fei.com/products/tem/tecna/> (accessed September 20, 2013).
- [7] Stouwdam JW, Shan J, van Veggel FCJM, Pattantyus-Abraham AG, Young JF, Raudsepp M. Photostability of colloidal PbSe and PbSe/PbS core/shell nanocrystals in solution and in the solid state. *J. Phys. Chem. C*, **2007**, 111, 1086-1092.
- [8] Dai Q, Wang Y, Zhang Y, Li X, Li R, Zou B, Seo JT, Wang Y, Liu M, Yu WW. Stability study of PbSe semiconductor nanocrystals over concentration, size, atmosphere, and light exposure. *Langmuir*, **2009**, 25, 12320–12324.
- [9] Hyun B, Chen H, Rey DA, Wise FW, Batt CA. Near-Infrared fluorescence imaging with water-soluble lead salt quantum dots. *J. Phys. Chem. B*, **2007**, 111, 5726-5730.

CHAPTER 3

3 Results and discussion

In this chapter, the results that were obtained during the synthesis and characterization of PbSe quantum dots are presented and discussed. The results mainly focus on the optical and morphological characterization of the synthesized nanocrystals. The optical characterization was carried out by monitoring the emission profiles of the nanocrystals using photoluminescence spectroscopy. The morphological characterization was done to elucidate structural information of the nanocrystals. The shapes of the nanocrystals were established from TEM micrographs. Nanocrystal sizes were obtained by measuring the images on the TEM micrographs using ImageJ software. X-ray diffraction patterns were used together with selected area electron diffraction (SAED) patterns to confirm the crystal structure of the synthesized nanocrystals.



3.1 Synthesis of PbSe QDs in organic media

The formation of QDs in colloidal solutions occurs majorly in two distinct stages i.e. nucleation and growth stages. These stages were extensively discussed by Murray *et al.* [1] and Viswanatha and Sarma [2]. In brief, the nucleation stage occurs when there is a sudden supersaturation of monomers in solution resulting in the formation of nuclei in a short period of time. This lowers the concentration of monomers in solution till they are insufficient to form new nuclei, the remaining monomers can only add to existing nuclei which occurs during the growth stage. With increased growth time, smaller particles dissolve in solution and the material is deposited on larger QDs through a process known as Ostwald ripening [1]. Murray *et al.* attribute Ostwald ripening to high surface energies on the smaller QDs, a process which is enhanced by high solution temperatures [1].

In this study the effects of reaction temperature, solvent, ligand purity, lead and selenium sources on the optical and structural properties of the synthesized PbSe QDs were investigated. The growth rate was monitored using photoluminescence (PL) spectroscopy while the size and shape were determined from transmission electron microscope (TEM) micrographs. The optimized conditions obtained were adopted for the investigation of the rest of the parameters which were under investigation.

3.1.1 Effect of temperature on the optical properties of PbSe QDs

Temperature plays a major role in the growth and size distribution of nanocrystals. Different groups have reported on the synthesis of lead chalcogenide QDs at temperatures between 80 °C and 220 °C [3], this work sought to determine the effects of these temperatures on the growth and properties of the QDs. The effect of temperature on the optical properties of PbSe QDs was investigated by carrying out similar reactions at different temperatures i.e. 90 °C, 120 °C and 150 °C. The lower temperatures were set at 90 °C and 120 °C based on previous reports which have reported on spherical QDs being obtained between 80 °C and 120 °C [3]. The highest temperature was set at 150 °C due to limitations during the optical characterization of QDs synthesized at higher temperatures. Ostwald ripening which influences QD growth and mainly depends on the reaction temperature was used to explain the observed optical changes.

At 90 °C the growth of nanocrystals was much relatively slow with Ostwald ripening occurring at a slow rate due to the low temperatures [1]. The nanocrystals were allowed to grow for a maximum of 30 min after which a uniform size distribution was attained as shown by the narrowing of the photoluminescence spectra (**Figure 3.1**). The QDs produced had a maximum emission at 1585 nm and an average size of 3.20 ± 0.4 nm (**Figure 3.2**). During the early stages in the growth of the PbSe QDs a large shift of approximately 203 nm (2-

4min) was observed in the PL spectra indicating the size evolution of the QDs. With increase in growth time the shifts were observed to decrease with the shift decreasing tenfold to approximately 19 nm between 20 min and 30 min. These smaller shifts imply that the QD size stabilizes with increasing growth time.

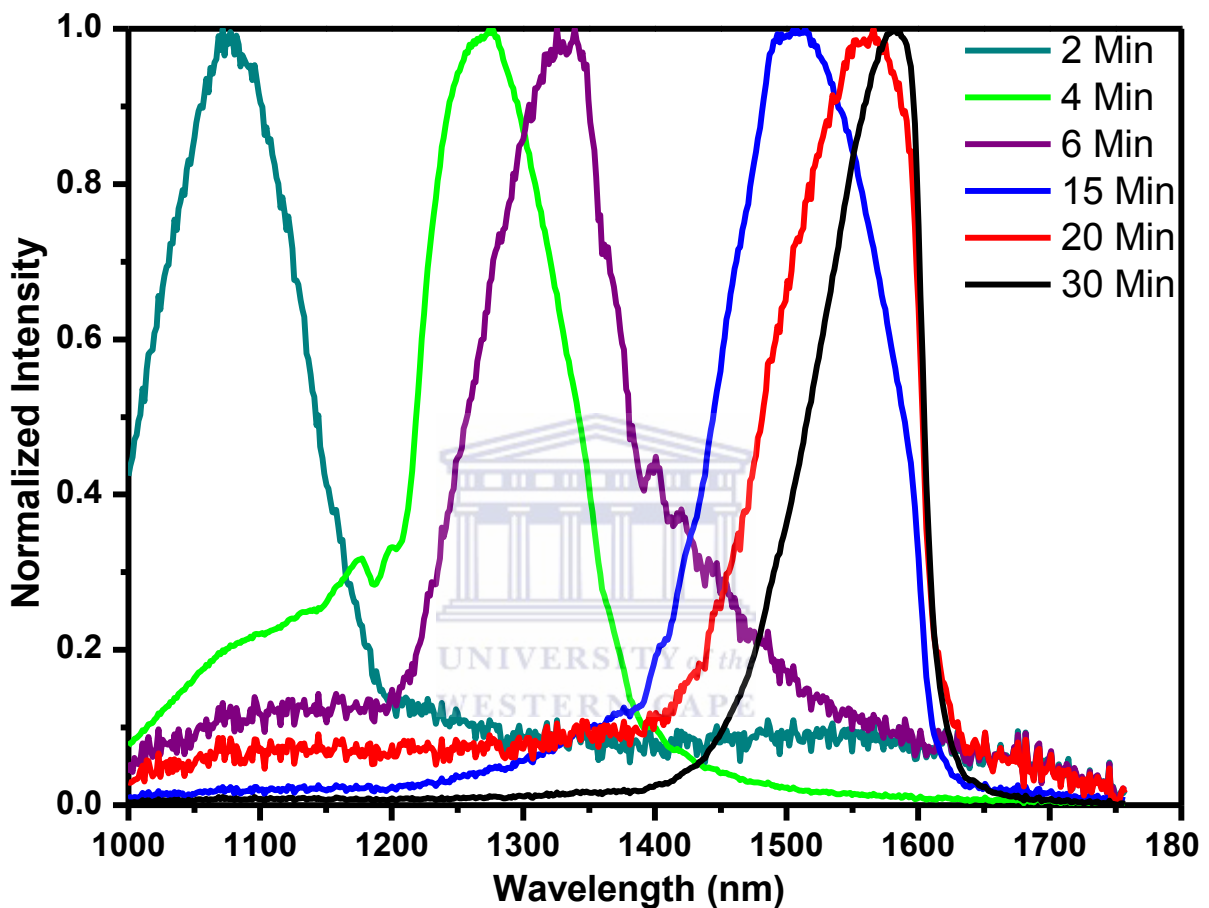


Figure 3.1 PL spectra of PbSe QDs aliquots taken during synthesis at 90 °C

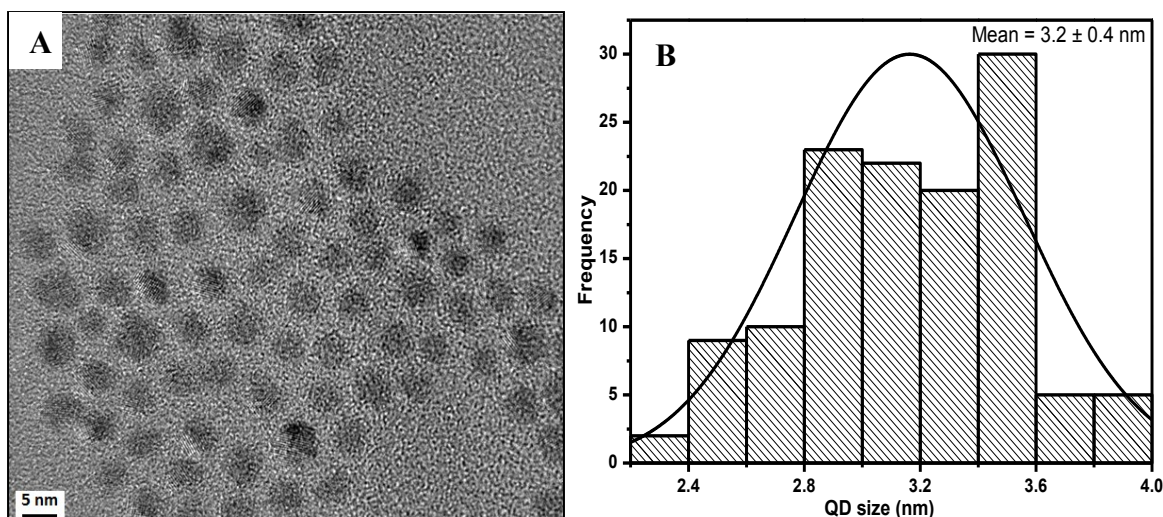


Figure 3.2 (A) TEM micrograph and (B) size distribution of PbSe QDs synthesized at 90 °C

At 120 °C the reaction took only 10 min to come to completion due to the higher reaction temperatures. Ostwald ripening was observed to take place at this reaction temperature but with more distinct growth phases. At this temperature the QD peaks were red shifted with increase in growth time indicating the size evolution of the QDs (**Figure 3.3**). After approximately 10 min the peaks overlap with a maximum emission of approximately 1585 nm implying that the QD growth had stopped. This maximum emission wavelength is similar the maximum emission wavelength of QDs synthesized at 90 °C. The QDs synthesized at this temperature had an average size of 3.65 ± 0.6 nm (**Figure 3.4**). These sizes are comparable to those obtained at 90 °C with reaction a reaction time of 30 min.

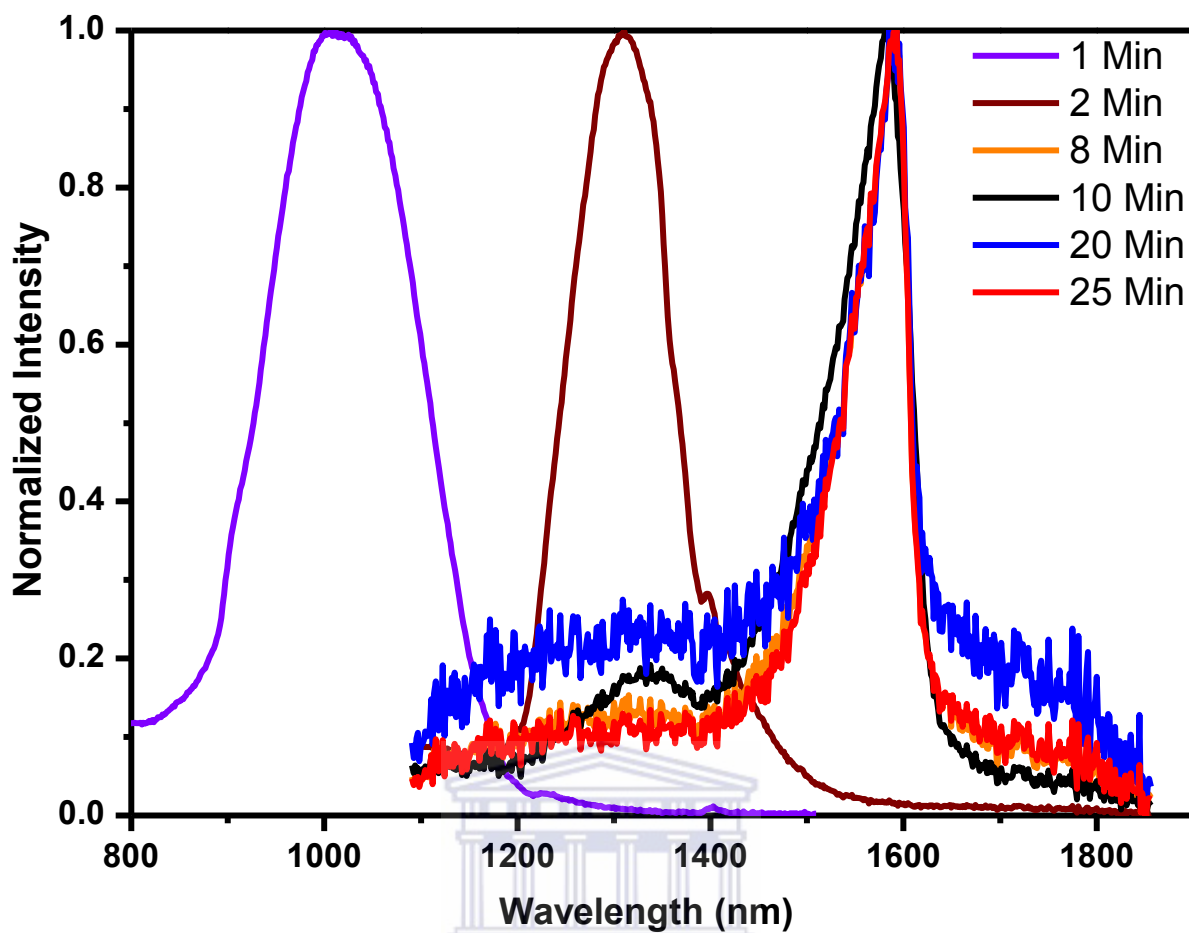


Figure 3.3 PL spectra of PbSe QDs aliquots taken during synthesis at 120 °C

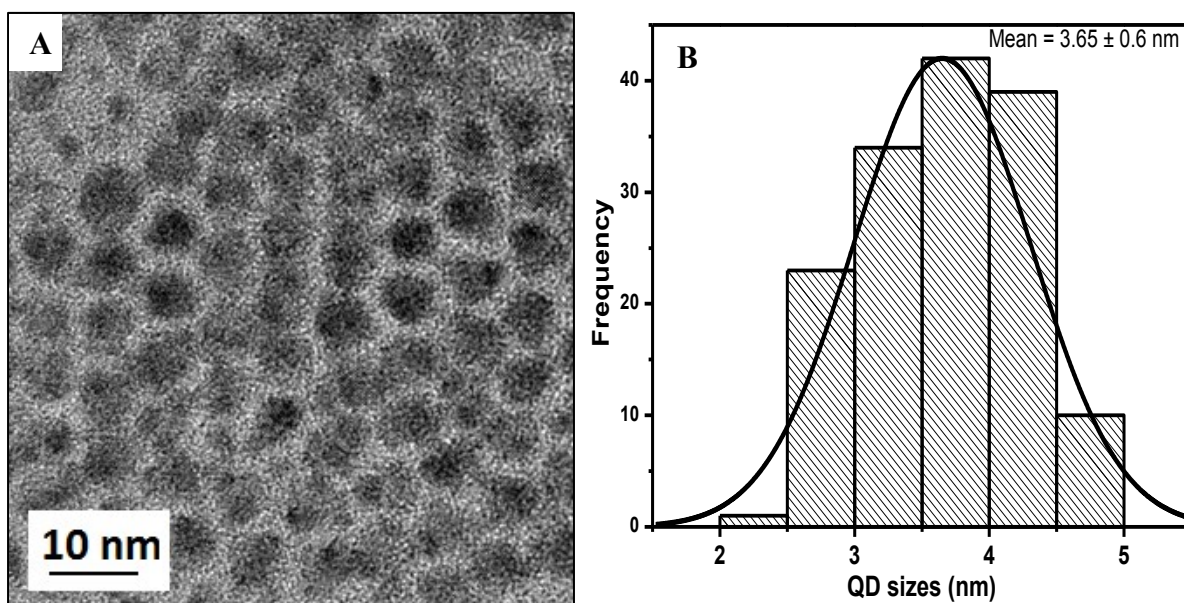
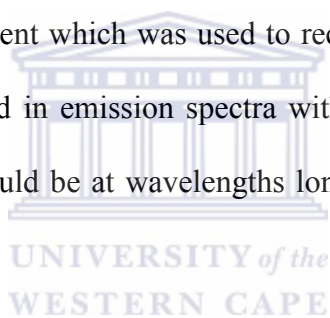


Figure 3.4 (A) TEM micrograph and (B) size distribution of PbSe QDs synthesized at 120 °C

At 150 °C the reactions progressed fairly fast with the NC growth stagnating within less than 10 min after the injection of the selenium precursor. During the earlier stages of NC growth, it could be observed from the PL spectra (**Figure 3.5**) that smaller QDs coexisted in solution with the larger ones as seen from the multiple emission peaks in the PL spectra. As the growth continued, the peaks at lower wavelengths (smaller articles) declined while those peaks at longer wavelengths (larger particles) were red shifted (**Figure 3.5**). This implies that the smaller QDs are dissolved as material adds to the larger particles. This is an indication of Ostwald ripening taking place. PbSe QDs were allowed to grow for a maximum of 15 min resulting in cubic QDs with average sizes of 14.8 ± 2.4 nm (**Figure 3.6**). The emission spectra of the PbSe QDs after 8 min growth time were not recorded due to limitations of the detector on the NanoLog instrument which was used to record the PL spectra. It is however possible to project from the trend in emission spectra with growth time that the maximum emission for these large QDs would be at wavelengths longer than those observed at 90 °C and 120 °C.



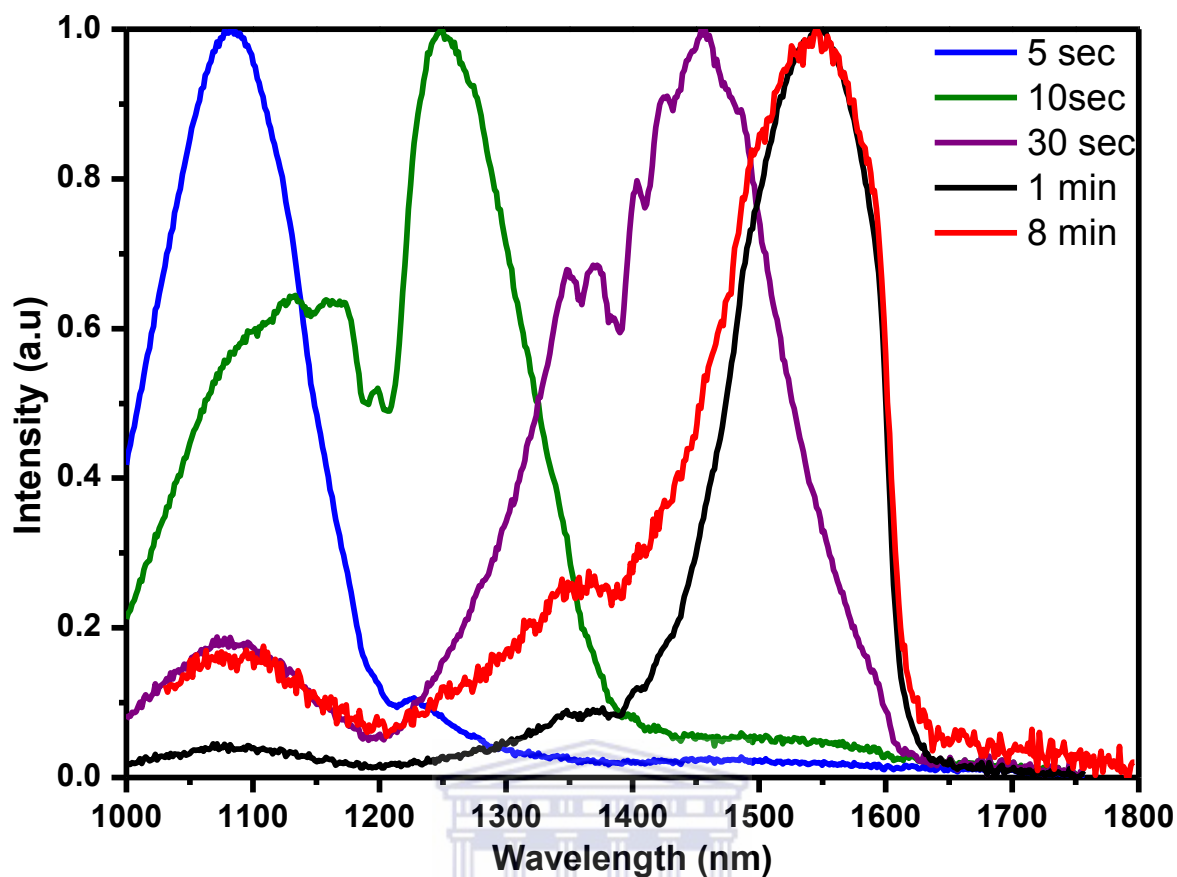


Figure 3.5 PL spectra of PbSe QDs aliquots taken during synthesis at 150 °C

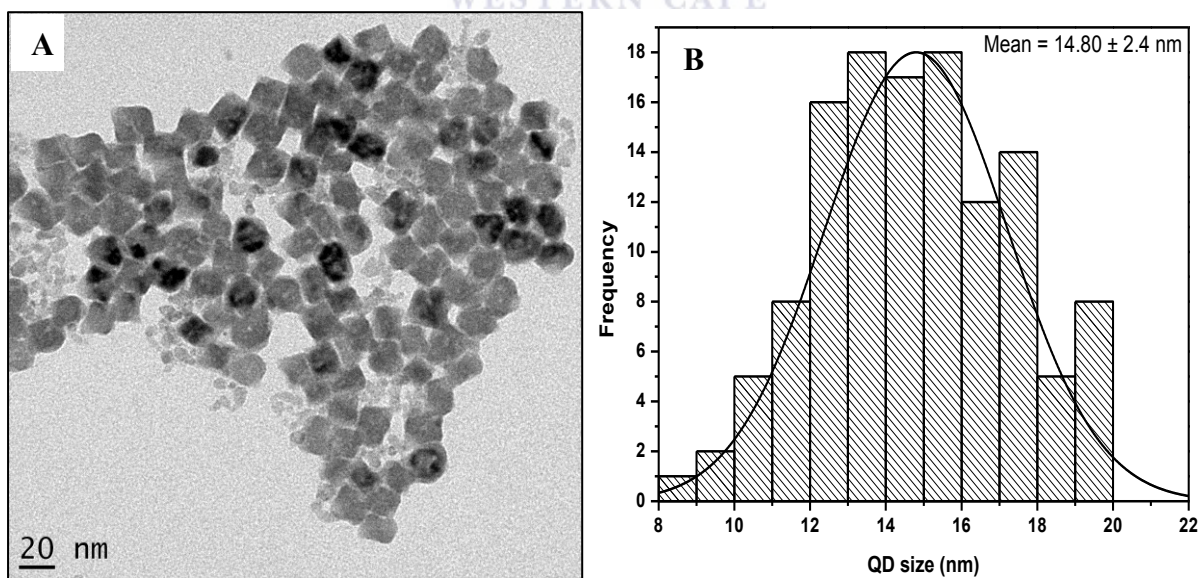


Figure 3.6 (A) TEM micrograph and (B) size distribution of PbSe QDs synthesized at 150 °C

At higher temperatures the growth of QDs occurred rapidly as shown by the red shift in emission spectra over time. Dai *et al.* [4] observed a similar growth trend at 140 °C while observing the shift in emission spectra. Higher reaction temperatures accelerate the chemical reaction producing a burst of nucleation. With an increase in growth time at high reaction temperatures, the formed nuclei agglomerate into octahedrons which with the addition of monomers grow into nanocubes as was observed by Lu *et al.* [5]. At higher reaction temperatures, ligands are more likely to desorb from the surface of QDs allowing monomers to add to NC surface resulting in bigger sized QDs [1]. Murray *et al.* reported that PbSe QDs are able to grow even at relatively low temperatures with solution temperatures being used to tune the QD size from 3.5 nm at 90 °C to 15 nm at 220 °C [1].

At lower reaction temperatures, a narrowing of emission spectra was observed corresponding to a narrower size distribution. The narrower size distribution was further confirmed from the reduction of full width at half maximum (FWHM) with decreasing temperatures (**Figure 3.7**). FWHM was observed to be 115.4 nm, 101.3 nm and 89.6 nm at 150 °C, 120 °C and 90 °C respectively. The control of size and size distribution of QDs can be attributed to crystal focussing which is hampered by fast growth of QDs [4]. The emission is however observed to stagnate at approximately 1600 nm at all the temperatures with maximum emissions of 1543 nm at 150 °C, and 1585 nm at 120 °C and 90 °C. This stagnation occurred faster at higher temperatures occurring after 30 min, 10 min and 8 min at 90 °C, 120 °C and 150 °C respectively (**Figure 3.8**). This could be attributed to depletion of starting materials or the reaction equilibrium having been reached and the QDs having reached their critical size [4].

It can therefore be concluded that of the investigated temperatures, 90 °C is the best temperature for the synthesis of PbSe nanocrystals under these reaction conditions for the intended studies. All the remaining effects were therefore investigated at 90 °C. At this reaction temperature PbSe QDs were synthesized at an average growth rate minimizing the

effects of Ostwald ripening and a uniform size distribution was attained as seen from the FWHM value since it gave the lowest value. These observations can be explained by the LaMer's theory in which the various growth stages are explained [6]. In this model, the supersaturation of species is relieved by a rapid burst of nucleation followed by a growth stage in which diffusing materials add to the existing nuclei. This leads to the depletion of monomers in solution thus decreasing the rate of nucleation resulting in a narrow size distribution [7]. According to LaMer and Dinegar, lowering the solution temperature can be used to adjust the solution concentration to provide a brief outburst leaving enough material for diffusional growth which results in a monodispersed formulation [6]. The shape of the photoluminescence spectrum was an almost perfect Gaussian shape which confirms that the nanocrystals had a pure band gap emission [8].

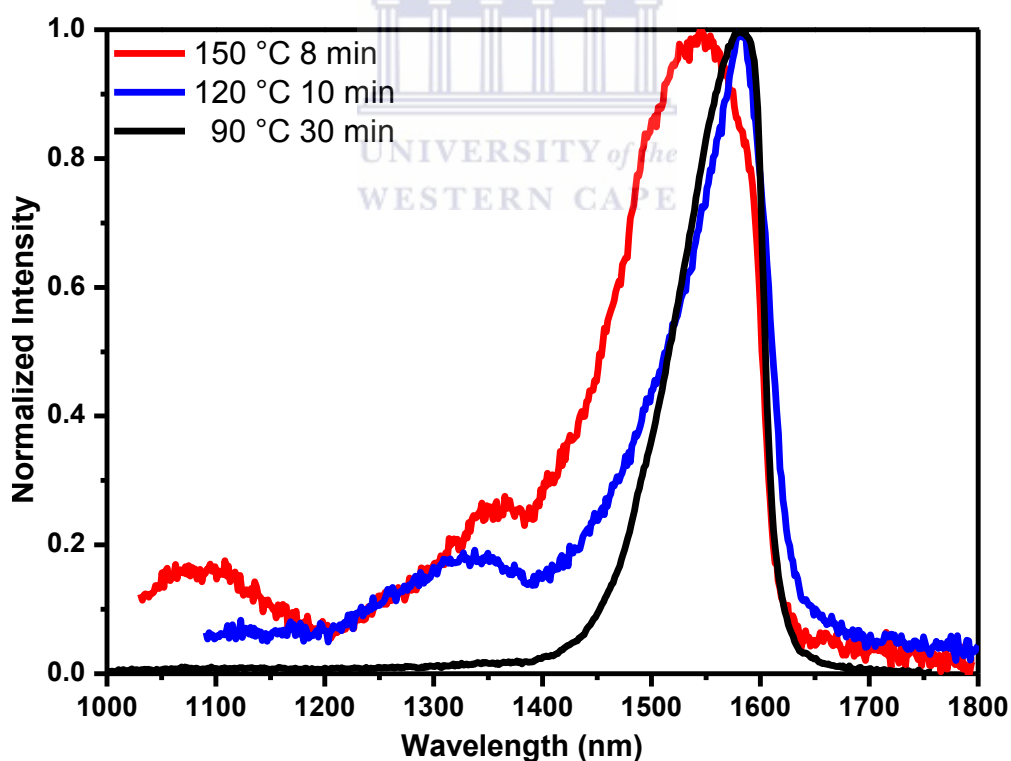


Figure 3.7 Emission spectra of QDs synthesized at different reaction temperatures

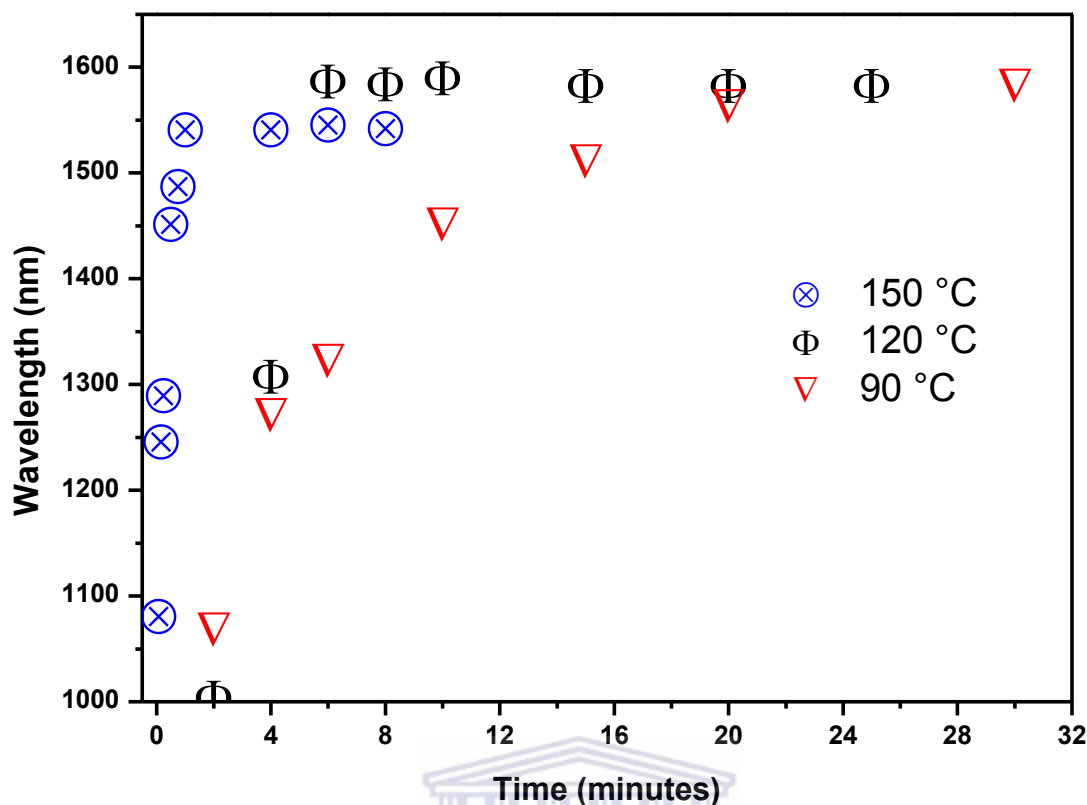


Figure 3.8 Summary of emission maxima with time at different reaction temperatures

3.1.2 Solvent effects on the optical and structural properties of PbSe QDs

The type of solvent used during a chemical reaction has significant bearings on the reaction kinetics. The Gibbs-Thompson thermodynamic equation and Ostwald ripening are dependent on the reactant concentrations which is a factor controlled by the solvent [9]. Most of the reported colloidal syntheses make use of the noncoordinating solvent 1-octadecene (ODE) or diphenyl ether. 1-Octadecene is preferred because of its high boiling point and noncoordinating nature, which allows the tuneable reactivity of monomers which in turn leads to a better control of NC sizes [1,10]. This property makes it relatively easier to determine the reaction kinetics of NC formation. Coordinating solvents mainly trioctylphosphine oxide (TOPO) have been used for group II-VI NC synthesis [11]. In this work different solvents were used in the growth of PbSe QDs.

Under similar reaction conditions, 1-octadecene (ODE) exhibited the fastest growth rate and produced the largest QDs compared to the other solvents as observed from the emission profiles (**Figure 3.9**). This can be attributed to its noncoordinating nature which implies that it does not influence the reaction. On the other hand, diphenyl ether produced the smallest sized particles with a much slower reaction rate as seen from the emission peaks (**Figure 3.9**). The lower boiling point and higher melting point of diphenyl ether may have contributed to the loss of monomers during vacuum drying of lead precursors since some of the solvent evaporated from the reaction mixture and condensed inside the condenser. This resulted in having fewer monomers for the QD growth hence resulting in smaller QDs. Trioctylphosphine (TOP), a coordinating solvent, produced medium sized QDs with an average growth rate as observed from the progression in QD emission profiles (**Figure 3.10**). TOP when used as a solvent may inhibit nucleation and growth of QDs by slowing the selenium exchange between trioctylphosphine selenide and lead oleate to form PbSe QDs [12]. Trioctylphosphine showed similar results to 1-octadecene but with smaller QDs being produced. The other solvent oleylamine which acts as both a solvent and surfactant [13] showed the slowest growth rate among the solvents investigated. The relatively slow growth rate and smaller QDs produced in oleylamine (**Figure 3.11**), compared to octadecene can be attributed to the activation of metal species by oleylamine which promotes nucleation leading to a higher number of nuclei and few monomers remaining in solution for the growth stage [13].

From the investigated solvents, it was observed that 1-octadecene (ODE), provided least interference to the QD nucleation and growth due to its noncoordinating nature, high boiling point and low melting point. Diphenyl ether lead to the loss of monomers due to its low melting point, trioctylphosphine hampered the exchange of selenium during the formation of

QDs while oleylamine led to the activation of metallic species. The subsequent reactions were therefore carried out in ODE.

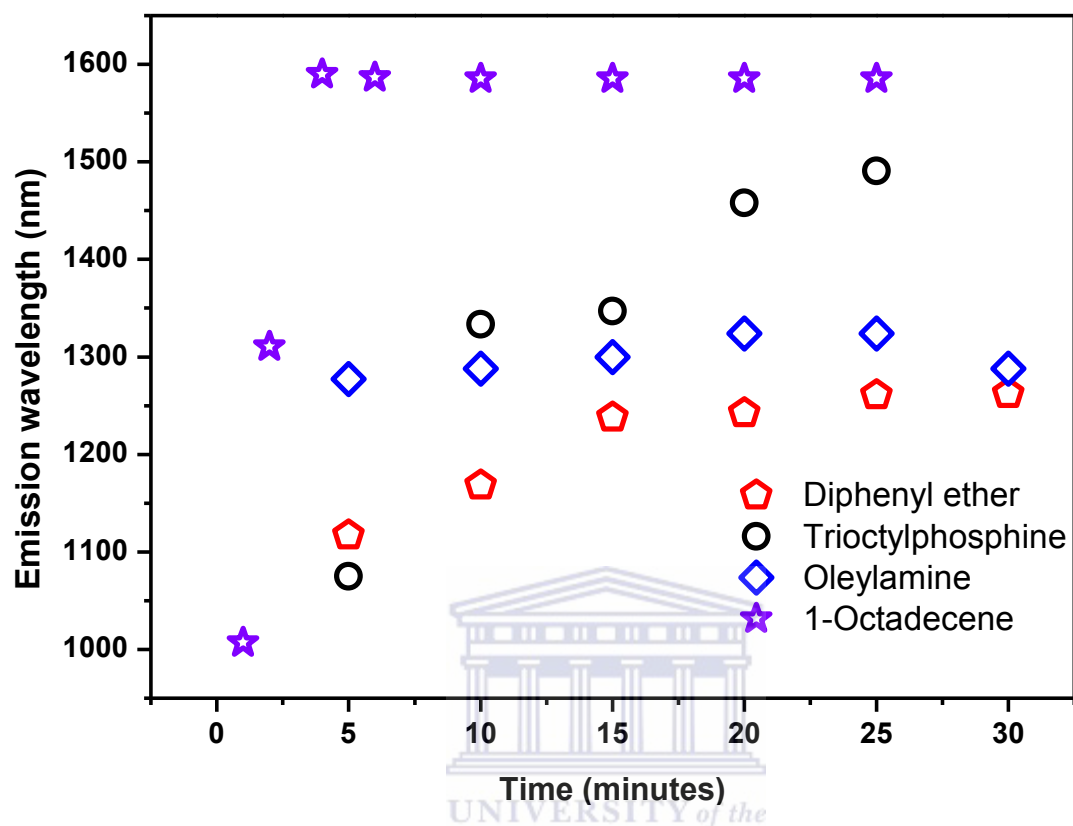


Figure 3.9 Summary of emission maxima with time in different solvents

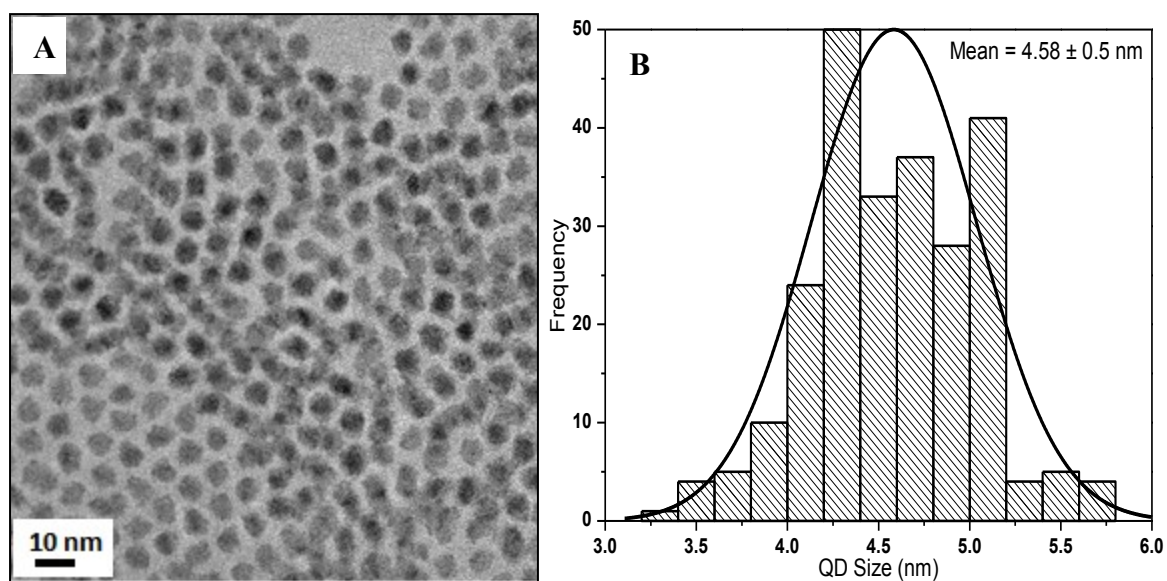


Figure 3.10 (A) TEM micrograph and (B) size distribution of PbSe QDs synthesized with TOP as solvent

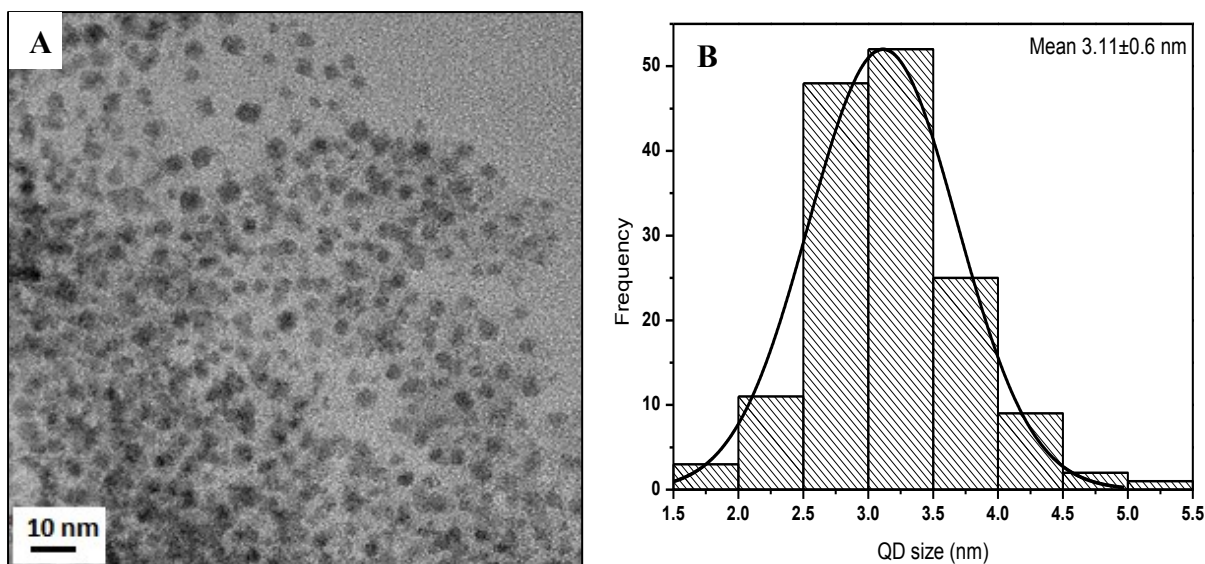


Figure 3.11 (A) TEM micrograph and (B) size distribution of PbSe QDs synthesized with OLA as solvent

3.1.3 Effect of ligand purity on the optical and structural properties of PbSe QDs

In this study it was observed that using 90 % and 99 % oleic acid in the synthesis of PbSe QDs produced crystals with relatively similar sizes, with the 90 % oleic acid producing QDs with slightly smaller sizes and a smaller size distribution (3.45 ± 0.3 nm) shown in **Figure 3.12** as compared to 99 % oleic acid (4.18 ± 0.5 nm) shown in **Figure 3.13**. The PbSe QDs synthesized using 90 % oleic acid provided relatively shorter emission wavelengths as compared to those synthesized from 99 % oleic acid (**Table 3.1**). The longer emission wavelengths are as a result of the relatively larger QD sizes. The purity of oleic acid therefore does not seem to have a similar influence on the QD size as the ligand/Pb ratios observed using DHLA [14]. Yu *et al.* investigated dihydrolipoic acid (DHLA) capped PbSe QDs and reported that decreasing DHLA/Pb molar ratios resulted in an increase in the PL intensity while at the same time shifting the emission peak to longer wavelengths [14].

Due to the smaller QD sizes and narrow size distribution obtained with 90 % oleic acid, it was considered the more appropriate ligand concentration to adopt in the subsequent reactions.

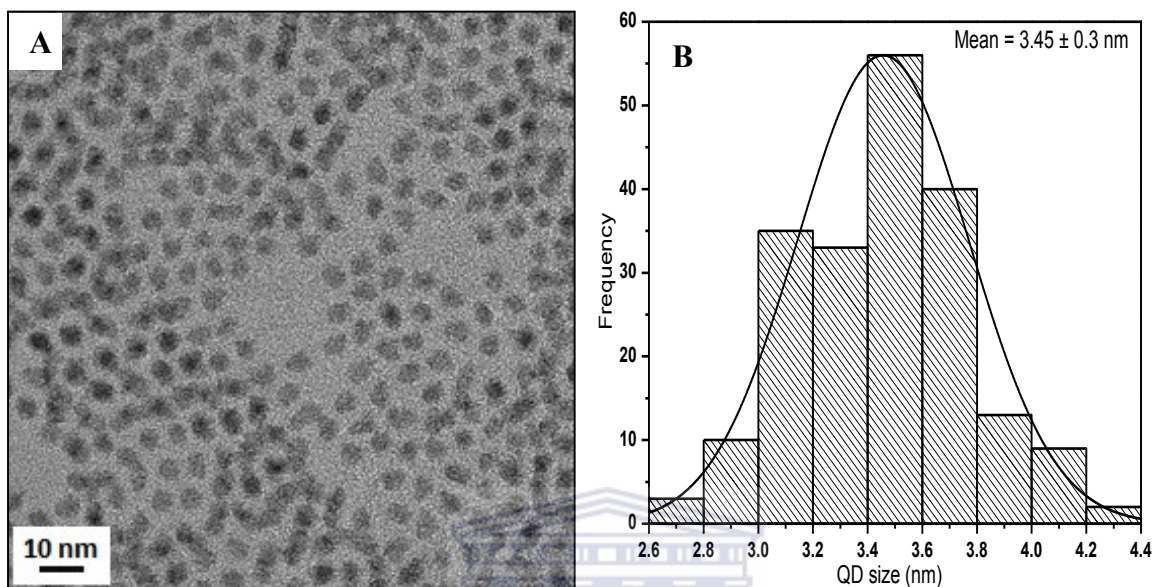


Figure 3.12 (A) TEM micrograph and (B) size distribution of PbSe QDs synthesized from PbO, TBPSe and 90 % oleic acid

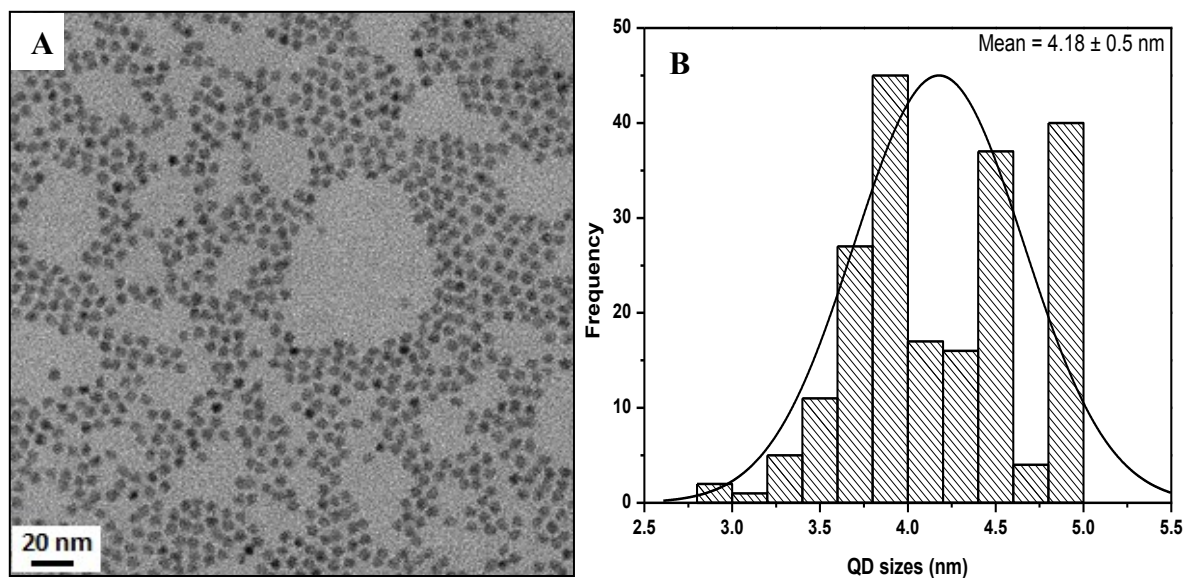


Figure 3.13 (A) TEM micrograph and (B) size distribution of PbSe QDs synthesized from PbO, TBPSe and 99 % oleic acid

Table 3.1 Effect of ligand purity on the optical and structural properties of PbSe QDs.

	Ligand	Pb source	Se source	Max. Emission	QD size
1.	90% OA	PbO	TBPS _e	1034 nm	3.45 ± 0.3 nm
2.	99% OA	PbO	TBPS _e	1263 nm	4.18 ± 0.5 nm

3.1.4 Effect of Lead and Selenium sources on the optical and structural properties of PbSe QDs

In these reactions lead oxide (PbO) and lead acetate (Pb(Ac)₂) were used as sources of lead atoms. Trioctylphosphine and tributylphosphine were used as ligands in the preparation of selenium precursors. PbSe QDs synthesized from lead oxide (**Figure 3.14**) gave monodispersed spherically shaped QDs. They were generally smaller compared to those synthesized from lead acetate (**Figure 3.15**). The QDs synthesized from lead acetate were cubic and agglomerated. The cubic shape can be attributed to the effects of free acetic acid which may result during the formation of lead oleate if there is residual water from the hydrated lead acetate [15]. Houtepen *et al.* provided great insight into the growth of PbSe QDs by investigating the effects of acetic acid on the growth of these nanocrystals [15]. They observed that if lead acetate is not completely dried before the injection of the chalcogen precursors, free acetate groups combine with water molecules (from the hydrated lead acetate) to form acetic acid. They investigated the effects of acetic acid on the growth of PbSe QDs following the addition of free acetic acid into the reaction mixture. They observed that addition of acetic acid influenced the size and shape evolution of QDs producing starlike QDs. Acetic acid being smaller than oleic acid partially replaces oleic acid on NC surfaces and due to the lower steric hindrance allows monomers to add to existing nuclei promoting growth in different directions.

Comparing the TEM micrographs of PbSe QDs synthesized using lead acetate and lead oxide, it was observed that the former produced cubic shapes (**Figure 3.15**) while the latter

produced predominantly spherical QDs (**Figure 3.14**). Lu *et al.* studied the shape evolution of PbSe QDs from spheres to octahedrons and finally cubes with increasing growth time and multiple injections of precursors [5]. Although their reactions were carried out at much higher reaction temperatures (180 °C and 230 °C) it is possible to conclude that a similar shape evolution took place in the reactions with lead acetate due to the presence of acetic acid as discussed earlier.

In QD synthesis, the ligand used on the chalcogen precursor also generally affects the size distribution of the QDs. In these reactions, trialkylphosphine selenides were used as selenium precursors. When comparing reactions using TOPSe and TBPSe, **Figure 3.14** and **Figure 3.16** respectively. TOPSe produced generally larger QDs as compared to TBPSe. This could be attributed to better size control by tributylphosphine as discussed below. Both tributylphosphine (TBP) and trioctylphosphine (TOP) form a P=Se double bond with selenium which is cleaved during nucleation when Se^{2-} ions react with Pb^{2+} ions to form QDs. The length of the alkyl chain indirectly affects the nucleation of the QDs but has not been shown to directly affect QD growth [4]. The longer TOP chain offers steric hindrance during the P=Se bond cleavage leading to the formation of fewer nuclei. TBP on the other hand favours the formation of nuclei leaving fewer monomers in solution for NC growth. This in turn leads to the formation of smaller QDs with a narrower size distribution [4].

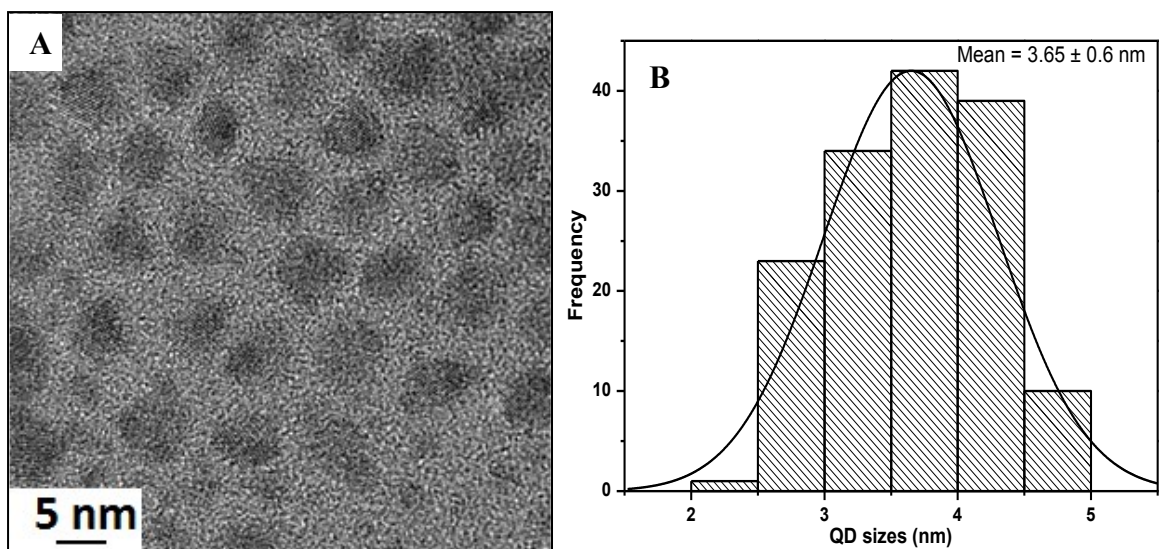


Figure 3.14 (A) TEM micrograph and (B) size distribution of PbSe QDs synthesized from PbO and TOPSe

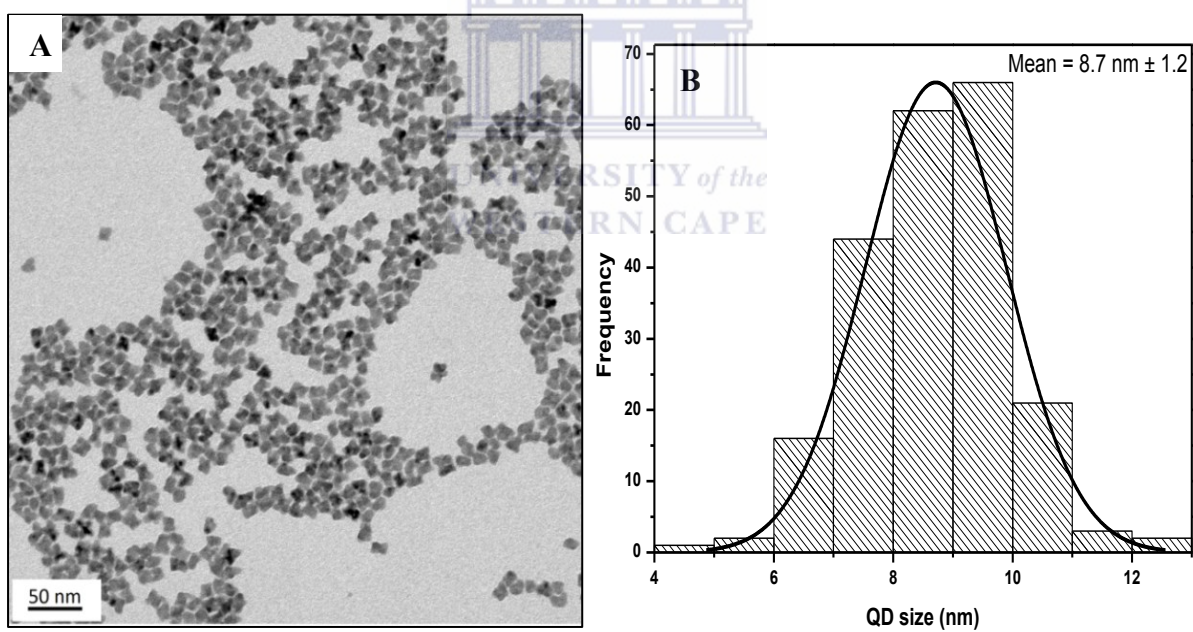


Figure 3.15 (A) TEM micrograph and (B) size distribution of PbSe quantum dots synthesized from Pb(Ac)₂ and TOPSe

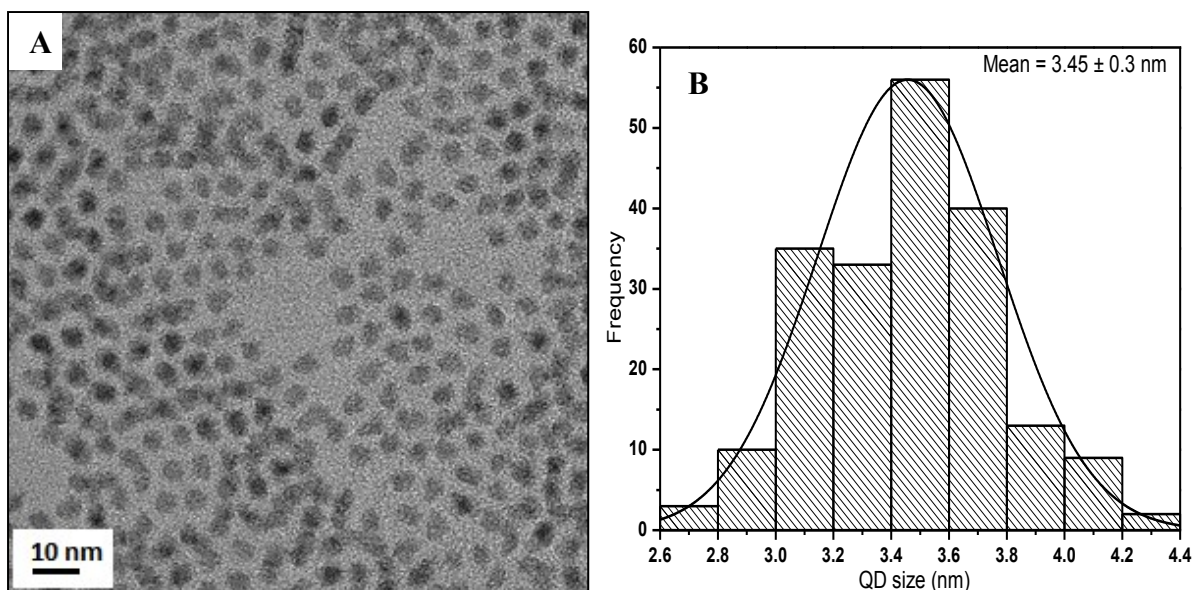


Figure 3.16 (A) TEM micrograph and (B) size distribution of PbSe quantum dots synthesized from PbO and TBPSe

3.1.4.1 Summary of the effects of lead and selenium sources on the optical and structural properties of PbSe QDs

The effects of lead and selenium sources on the optical and structural properties of PbSe QDs were investigated and the results summarized in **Table 3.2**. From the table it is evident that the QD sizes affect their optical properties with larger QDs generally providing longer emission wavelengths. **Figure 3.17** shows an EDS spectrum of some of the synthesized QDs, from the spectrum it can be confirmed that the synthesized PbSe QDs were indeed non-stoichiometric consisting of more lead atoms than selenium atoms as shown by the atomic percentages. This is consistent with reports that PbSe QDs are off-stoichiometric consisting of a stoichiometric PbSe core wrapped with a single layer of Pb atoms [16,17,18].

Table 3.2 Effect of lead and selenium sources on the optical and structural properties of PbSe QDs.

	Ligand	Pb source	Se source	Max. Emission	QD size
1.	OA	PbO	TOPSe	1320 nm	3.65 ± 0.6 nm
2.	OA	PbO	TBPS	1034 nm	3.45 ± 0.3 nm
3.	OA	Pb(Ac) ₂	TOPSe	1590 nm	8.7 ± 1.2 nm

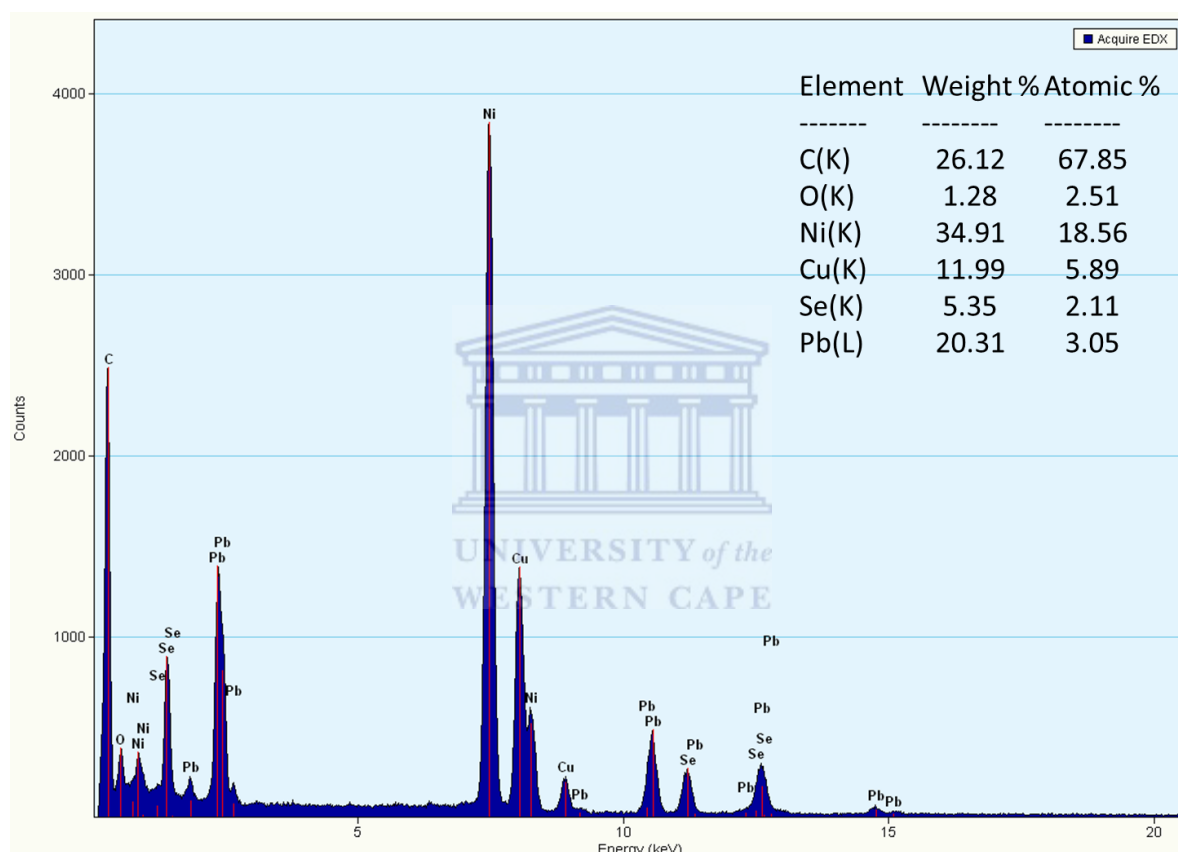


Figure 3.17 EDS spectrum of PbSe quantum dots

3.2 Ligand exchange of organic synthesized QDs

The synthesized QDs were transferred from organic to aqueous media through ligand exchange with 11-mercaptoundecanoic acid (MUA). Ligand exchange was attempted with 3-mercaptopropionic acid (MPA) but the reaction was unsuccessful with the QDs remaining in

the organic phase even after excess MPA was used. This could be a result of MPA not being able to displace oleic acid (OA) from the surface of PbSe QDs due to the instability of the Pb-thiolate bond [19]. Ligand exchange was then carried out with 11-mercaptoundecanoic acid which successfully transferred the QDs from the organic phase into the aqueous phase. Following the ligand exchange a blue shift was observed in the emission spectra of the PbSe QDs (**Figure 3.18**). The spectrum of the ligand exchanged QDs was observed to be narrower than that of the hydrophobic QDs (**Figure 3.18**). Hyun *et al.* observed a red shift when they exchanged oleic acid for MUA on the surface of PbSe and PbS QDs [20]. They attributed the red shift to the change of electronic density and the confinement due to the Pb-thiol bond [20]. They also observed broadening of the QD emission spectrum after ligand exchange. Experiments have shown that PbSe QDs consist of a PbSe core surrounded by Pb atoms onto which oleic acid molecules are bound [17,18]. When the QDs are oxidised, desorption of oleic acid from the NC surface and the bonded Pb surface atoms occurs leading to QD shrinkage [4,17]. The blue shift and narrowing of the emission spectrum observed could therefore be attributed to the desorption of oleic acid and bonded Pb surface atoms following oxidation since the ligand exchange reaction was carried out in air [17].

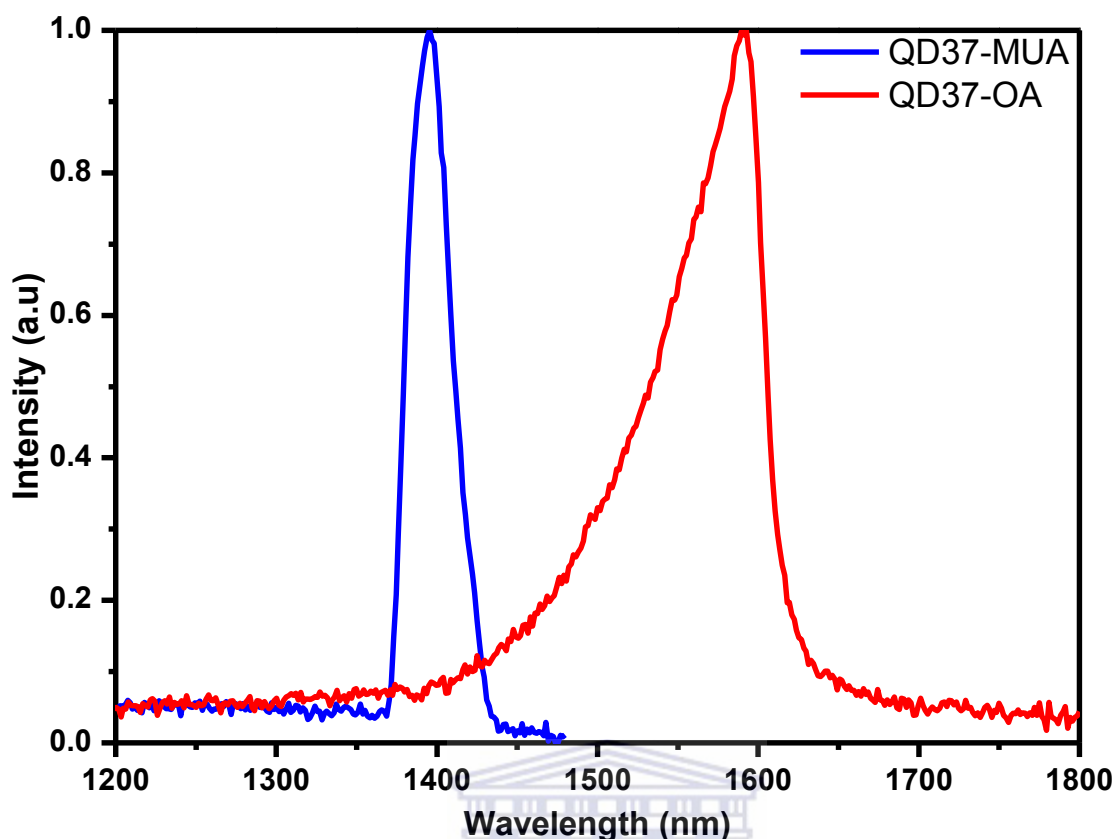


Figure 3.18 PL spectra of oleic acid-capped QDs (QD37-OA) and 11-mercaptoundecanoic acid-capped QDs (QD37-MUA) following ligand exchange.

3.3 Synthesis of PbSe QDs in aqueous media

These results have been published in [21].

Aqueous synthesis of PbSe QDs was carried out at room temperature as explained in the experimental section. Pb^{2+} ions were obtained by dissolving lead acetate trihydrate in deionized water in the presence of 3-mercaptopropionic acid which acted as the surfactant during the quantum dot synthesis. Se^{2-} ions were introduced in the form of H_2Se gas. PbSe nanocrystals started forming immediately the H_2Se gas was transferred into the flask containing the Pb precursor. This observation showed that Pb^{2+} ions reacted rapidly with Se^{2-} in aqueous solutions at room temperature. A similar observation was reported by Li *et al.* during the synthesis of citrate-capped nanocrystals [22].

The synthesized QDs were capped with 3-mercaptopropionic acid which is a shorter chained ligand compared to oleic acid which is commonly used in the synthesis of PbSe QDs. Apart from offering the solubility of the QDs in aqueous media, the short chained MPA promotes the application of these QDs in photovoltaic cells and light emitting diodes by promoting charge separation at the nanocrystal surface [23]. The rate of energy transfer for electroluminescence has been attributed to both the capping ligand and proximity between the exciton donor and acceptor where shorter ligands have been shown to give a significant improvement in excitation-transfer efficiency [24].

3.3.1 Photoluminescence properties

The PL spectrum of the as-synthesized PbSe QDs (**Figure 3.19**) is a perfect Gaussian shape as shown by the complete overlap of the Gaussian fit on the QD spectrum. This indicates a pure band gap emission with a FWHM of ~23 nm indicative of a narrow size distribution [8]. The emission peak position of 1203 nm (1.03 eV) similar to previously reported value (1205 nm) for oleic acid capped PbSe nanocrystals observed by Yu *et al.* in 2004 [4] but observably differs from 1107 nm (1.12 eV) reported by Sashchiuk *et al.* [25] for tributylphosphine-capped nanocrystals. This indicates the influence of different capping agents on the growth of PbSe QDs.

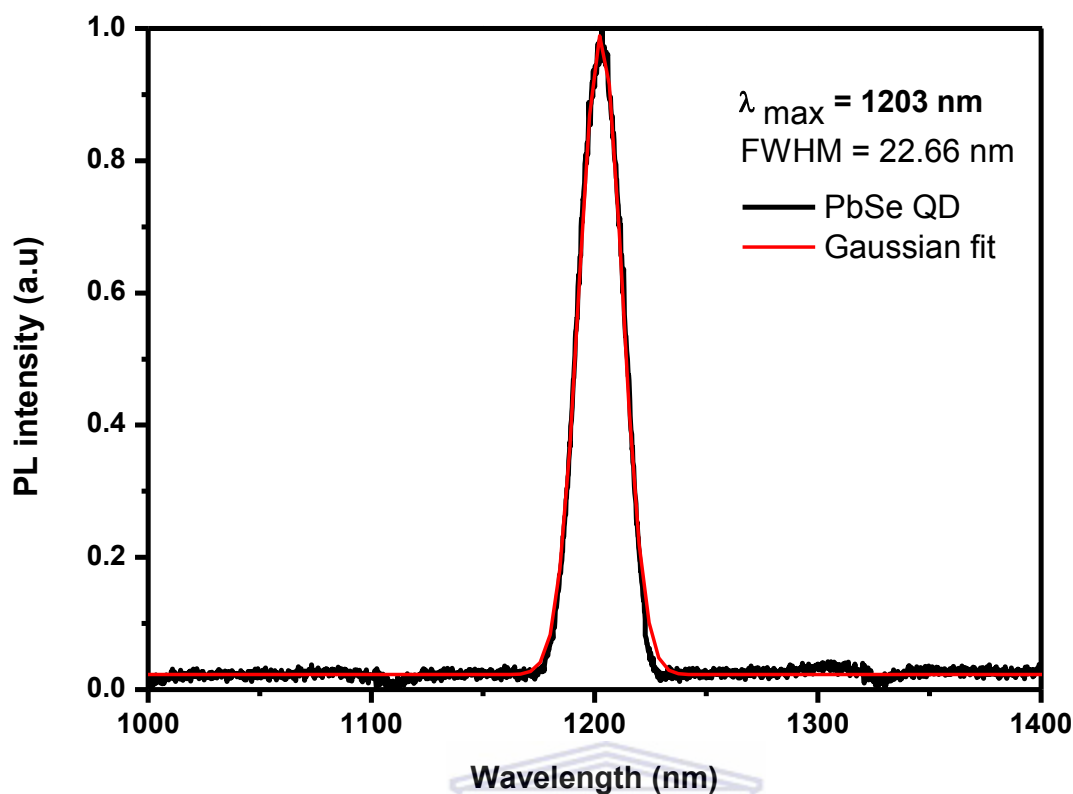


Figure 3.19 Normalized PL spectrum of MPA-capped PbSe QDs

Near-infrared emitting aqueous compatible QDs are highly valuable in terms of biological applications since most biological tissues are considered “transparent” in this region making it possible to image through several layers of tissue. These QDs are also known to have long fluorescence lifetimes allowing them to be applicable in long term imaging. The synthesized QDs were analysed and stored in deionised water. The QDs were however only stable in solution for 48 h when stored either in the dark at 4 °C or at ambient conditions. This could be attributed to the instability of the Pb-thiolate complex with Pb-S bond length of 2.7 Å and stability energy of -0.7903 a.u [19].

3.3.2 Structural properties

3.3.2.1 Transmission electron microscopy

The transmission electron microscopy (TEM) micrograph of the samples (**Figure 3.20**) reveals that the synthesized QDs are spherically shaped with an average diameter of 2.8 ± 0.2

nm. These measurements concur with the spectrum from PL which reveals a narrow peak and small FWHM. Lattice fringes observed in the high resolution transmission electron microscope (HR-TEM) micrographs revealed that the synthesized nanoparticles were highly crystalline in nature. The energy dispersive X-ray spectroscopy (EDS) spectrum of the QDs (**Figure 3.21**) confirmed that the synthesized QDs were indeed made up of lead atoms and selenium atoms. Carbon and oxygen atoms were also present on the spectrum possibly from the MPA molecules on the QD surface. QDs were analysed on a carbon coated copper grid which contributed to some of the carbon observed and the strong copper peak on the EDS spectrum. From the EDS spectrum it can be deduced that the QDs contain more lead atoms than selenium atoms. This selenium deficiency was discussed by Petkov *et al.* to be a result of the QD surface being terminated with lead atoms only [16]. They studied bulk PbSe and PbSe quantum dots of different sizes using high-energy x-ray diffraction coupled to atomic pair-distribution-function analysis and computer simulations. From their observations, they concluded that in PbSe QDs the Pb/Se ratio ranges between 1.30 to 1.75 for QDs with sizes between 2.8 nm and 6.2 nm respectively. From the EDS spectrum the atomic ratio of Pb/Se was calculated to be 1.64 for the synthesized QDs. A similar Pb/Se atomic ratio was found to correspond to 3.99 nm PbSe QDs by Dai *et al.* who calculated the ratios based on atomic absorption spectroscopy (AAS) data [26].

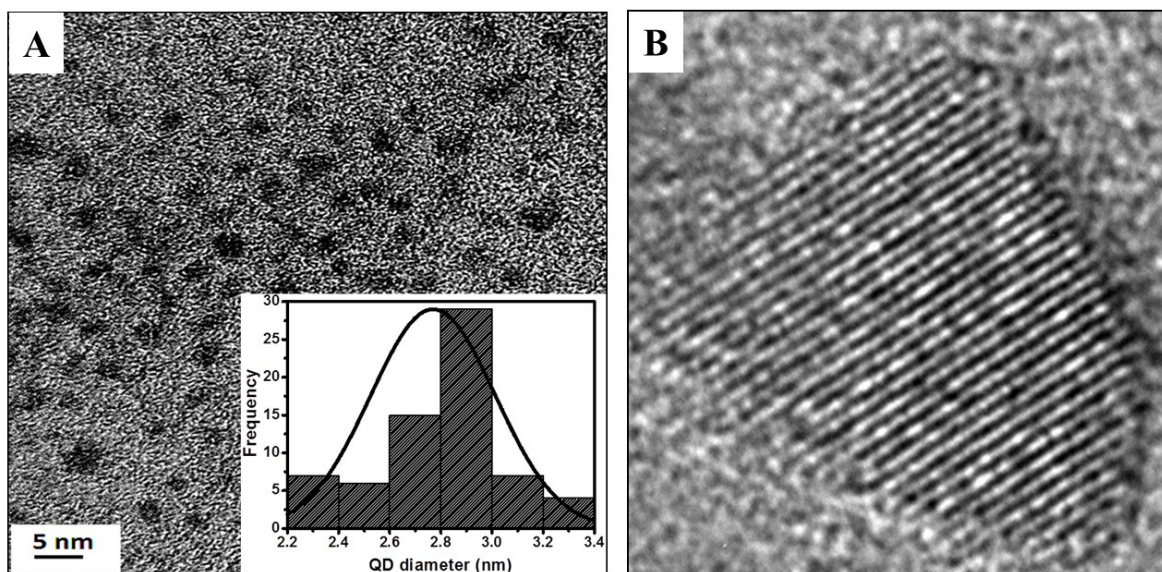


Figure 3.20 (A) TEM micrograph and (B) High resolution TEM image showing lattice fringes

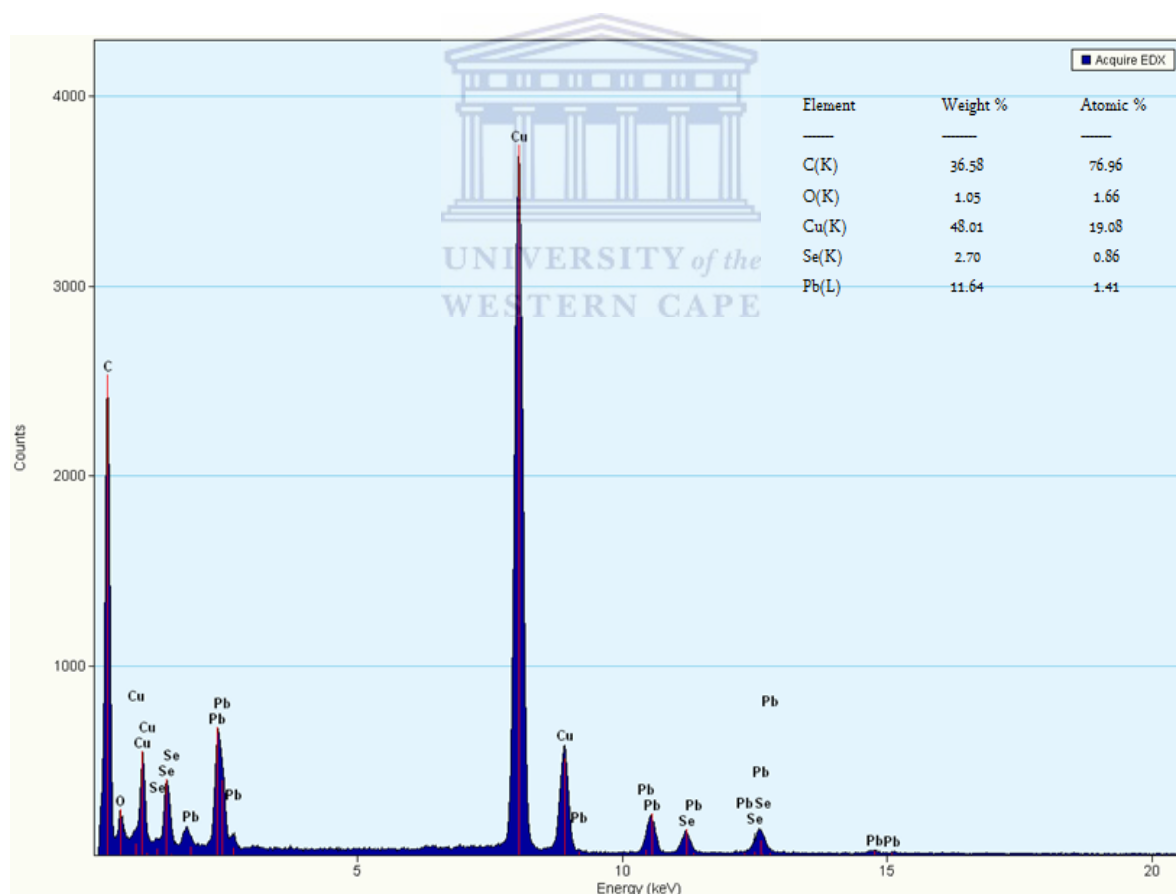


Figure 3.21 EDS spectrum of PbSe nanocrystals

3.3.2.2 X-ray diffraction patterns

XRD peaks were observed around 25.66° , 29.63° , 42.75° , 50.91° , 53.14° , 62.31° , 68.65° , 70.66° , and 78.77° which were fairly consistent with previously reported data corresponding to rock-salt cubic structured PbSe [22,27]. These peaks were assigned to crystal planes (111), (200), (220), (311), (222), (400), (331), (420), and (422) respectively (**Figure 3.22**). The SAED pattern showed diffraction rings consistent with a single rock-salt phase of the synthesised PbSe nanocrystals (**Figure 3.22 Inset**).

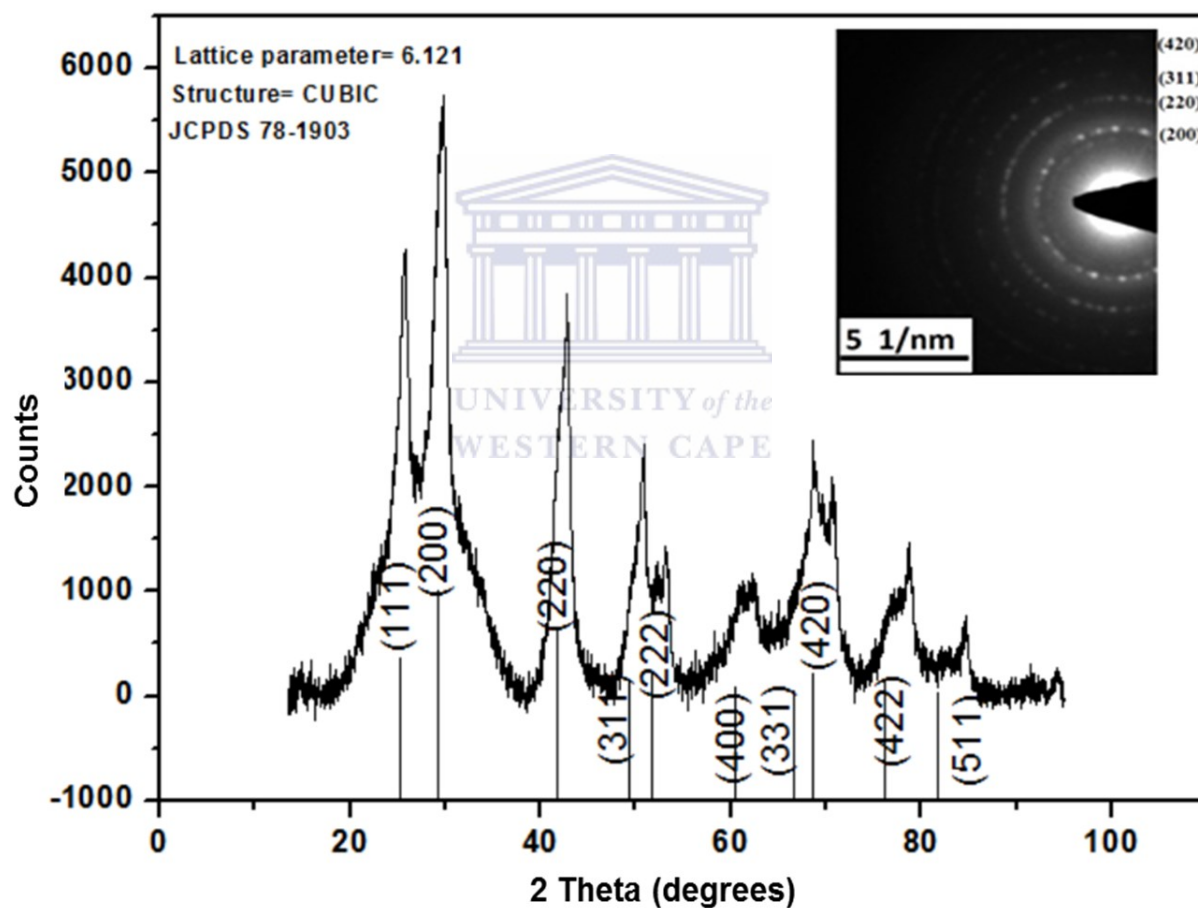


Figure 3.22 X-Ray diffractogram of MPA capped PbSe QDs
Inset: SAED Pattern of PbSe QDs with indexing of the main diffraction rings.

3.4 References

-
- [1] Murray CB, Sun S, Gaschler W, Doyle H, Betley TA, Kagan CR. Colloidal synthesis of nanocrystals and nanocrystal superlattices *IBM J. Res. Dev.*, **2001**, 45, 47-56.
- [2] Viswanatha R, Sarma DD. Growth of nanocrystals in solution. In Rao CNR, Müller A, Cheetham AK, editors. Nanomaterials chemistry: recent developments and new directions. *Weinheim, Germany; Wiley-VCH Verlag GmbH & Co. KGaA*, **2009**, p. 139-170.
- [3] Gokarna A, Jun K, Khanna PK, Baeg J, Seok SI, Colloidal synthesis of octahedral shaped PbSe nanocrystals from lead oleate and Se : Temperature effect. *B. Korean Chem. Soc.* **2005**, 26, 1803-1806.
- [4] Dai Q, Zhang Y, Wang Y, Wang Y, Zou B, Yu WW, Hu MZ. Ligand effects on synthesis and post-synthetic stability of PbSe nanocrystals. *J. Phys. Chem. C*, **2010**, 114, 16160–16167.
- [5] Lu W, Fang J, Ding Y, Wang ZL. Formation of PbSe nanocrystals: a growth toward nanocubes. *J. Phys. Chem. B*, **2005**, 109, 19219-19222.
- [6] LaMer VK, Dinegar RH. Theory, production and mechanism of formation of monodispersed hydrosols. *J. Am. Chem. Soc.* **1950**, 72, 4847-4848.
- [7] Robb DT, Privman V. Model of nanocrystal formation in solution by burst nucleation and diffusional growth. *Langmuir*, **2008**, 24, 26-35.
- [8] Yu WW, Falkner JC, Shih BS, Colvin VL. Preparation and characterization of monodisperse PbSe semiconductor nanocrystals in a noncoordinating solvent. *Chem. Mater.*, **2004**, 16, 3318.
- [9] Nishioka K, Maksimov IL. Reconsideration of the concept of critical nucleus and the Gibbs-Thomson equation. *J. Cryst. Growth*, **1996**, 163, 1-7.

-
- [10] Yu WW, Peng X. Formation of high-quality CdS and other II-VI semiconductor nanocrystals in noncoordinating solvents: tunable reactivity of monomers. *Angew. Chem. Int. Ed.*, **2002**, 41, 2368-2371.
- [11] Sowers KL, Swartz B, Krauss TD. Chemical mechanisms of semiconductor nanocrystal synthesis. *Chem. Mater.*, **2013**, 25, 1351-1362.
- [12] Evans CM, Evans ME, Krauss TD. Mysteries of TOPSe revealed: insights into quantum dot nucleation. *J. Am. Chem. Soc.*, **2010**, 10973-70975.
- [13] Jin X, Parisi J, Kolny-Olesiak J. Shape control of CdTe nanocrystals: influence of the solvent composition and ligand effects. *J. Nanopart.*, **2013**, 2013, 243831(7pgs)
- [14] Yu Y, Zhang K, Li Z, Sun S. Synthesis and luminescence characteristics of DHLA-capped PbSe quantum dots with biocompatibility. *Opt. Mater.*, **2012**, 34, 793–798.
- [15] Houtepen AJ, Koole R, Vanmaekelbergh D, Meeldijk J, Hickey SG. The hidden role of acetate in the PbSe nanocrystal synthesis. *J. Am. Chem. Soc.*, **2006**, 128, 6792–6793.
- [16] Petkov V, Moreels I, Hens Z, Ren Y. PbSe quantum dots: Finite, off-stoichiometric, and structurally distorted. *Phys. Rev. B*, **2010**, 81, 241304-1-241304-4.
- [17] Moreels I, Fritzinger B, Martins JC, Hens Z. Surface chemistry of colloidal PbSe nanocrystals. *J. Am. Chem. Soc.*, **2008**, 130, 15081-15086.
- [18] Moreels I, Lambert K, Muynck DD, Vanhaecke F, Poelman, Martins JC, Allan G, Hens Z. Composition and size-dependent extinction coefficient of colloidal PbSe quantum dots. *Chem. Mater.*, **2007**, 19, 6101-6106.
- [19] Primera-Pedrozo OM, Arslan Z, Rasulev B, Leszczynski J, Room temperature synthesis of PbSe quantum dots in aqueous solution: stabilization by interactions with ligands. *Nanoscale*, **2012**, 4, 1312-1320.

-
- [20] Hyun B, Chen H, Rey DA, Wise FW, Batt CA. Near-Infrared fluorescence imaging with water-soluble lead salt quantum dots. *J. Phys. Chem. B*, **2007**, 111, 5726-5730.
- [21] Ouma ILA, Mushonga P, Madiehe AM, Meyer M, Dejene FB, Onani MO. Synthesis, optical and morphological characterization of MPA-capped PbSe nanocrystals. *Physica B.*, <http://dx.doi.org/10.1016/j.physb.2013.10.057>.
- [22] Li J, Xu J, Zhao L, Xu Q, Fang G. Preparation and characterization of CdSe and PbSe nanoparticles via aqueous solution for nanoparticle-based solar cells. *Mater. Res. Bull.*, **2013**, 48, 1560-1568.
- [23] Xu J, Cui D, Zhu T, Paradee G, Liang Z, Wang Q, Xu S, Wang AY. Synthesis and Surface-Modification of PbSe/PbS Core-Shell Nanocrystals for Potential Device Applications. *Nanotechnology*, **2006**, 17, 5428-5434.
- [24] Sargent EH. Infrared quantum dots. *Adv. Mater.*, **2005**, 17, 515-522.
- [25] Sachiuk A, Langof L, Chaim R, Lifshitz E. Synthesis and characterization of PbSe and PbSe/PbS core-shell colloidal nanocrystals. *J. Cryst. Growth*, **2002**, 240, 431-438.
- [26] Dai Q, Wang Y, Li X, Zhang Y, Pellegrino DJ, Zhao M, Zou B, Seo J, Wang Y, Yu WW. Size-dependent composition and molar extinction coefficient of PbSe semiconductor nanocrystals. *ACS. Nano*, **2009**, 3, 1518-1524.
- [27] Niu J, Shen H, Li X, Xu W, Wang H, Li LS. Controlled synthesis of high quality PbSe and PbTe nanocrystals with one-pot method and their self-assemblies. *Colloid Surface A.*, **2012**, 406, 38

CHAPTER 4

4 Biological applications of PbSe quantum dots

Quantum dot toxicity has raised major concerns due to their heavy metal compositions [1,2,3]. The heterogeneous nature of QDs and their size dependent properties make it difficult to make generalizations about their nature including their toxicity [4]. QD toxicity has been attributed to several mechanisms including leaching of heavy metal ions following oxidation, intracellular degradation or both which cause hepatic cell death [5]. It has also been attributed to the generation of reactive oxygen species (ROS) which damage cellular proteins, lipids and deoxyribonucleic acid (DNA) [4].

PbSe nanocrystals synthesized in this study were mainly intended for diagnostic studies *in vitro*. The biological effects of the as-synthesized 11-mercaptopundecanoic acid-capped (MUA-capped) PbSe quantum dots were investigated following the water-soluble tetrazolium salt (WST-1) assay on human colorectal adenocarcinoma (Caco-2) cells. The synthesized MPA-capped PbSe quantum dots aggregated within less than 24 h therefore were not favourable for cytotoxicity tests since the experiment requires an incubation period of 24 h.

4.1 Results of preliminary cytotoxicity studies

The effect of PbSe QDs on Caco-2 cell viability was evaluated by WST-1 assay after exposure to PbSe QDs of various concentrations for 24 h as described in the experimental section (experiments were carried out in triplicate). The QDs tested were relatively non-toxic to the cells at all tested concentrations. Even at the highest tested concentration of 500 ng/mL, approximately 90 % of the cells were viable. The non-toxicity could be attributed to strong QD-ligand bonds which prevent the QDs from being oxidised. Oxidation of the QDs causes metal ions to leach into cells. **Figure 4.1** shows the effects of PbSe QDs on Caco-2

cell viability. Similar results were reported by Peng *et al.* for CdSe/ZnS QDs on human hepatocellular carcinoma cells. They exposed the cells to CdSe/ZnS QDs for 24 h. The study reported that the QDs were relatively less toxic as compared to both cadmium and selenium ions [6].

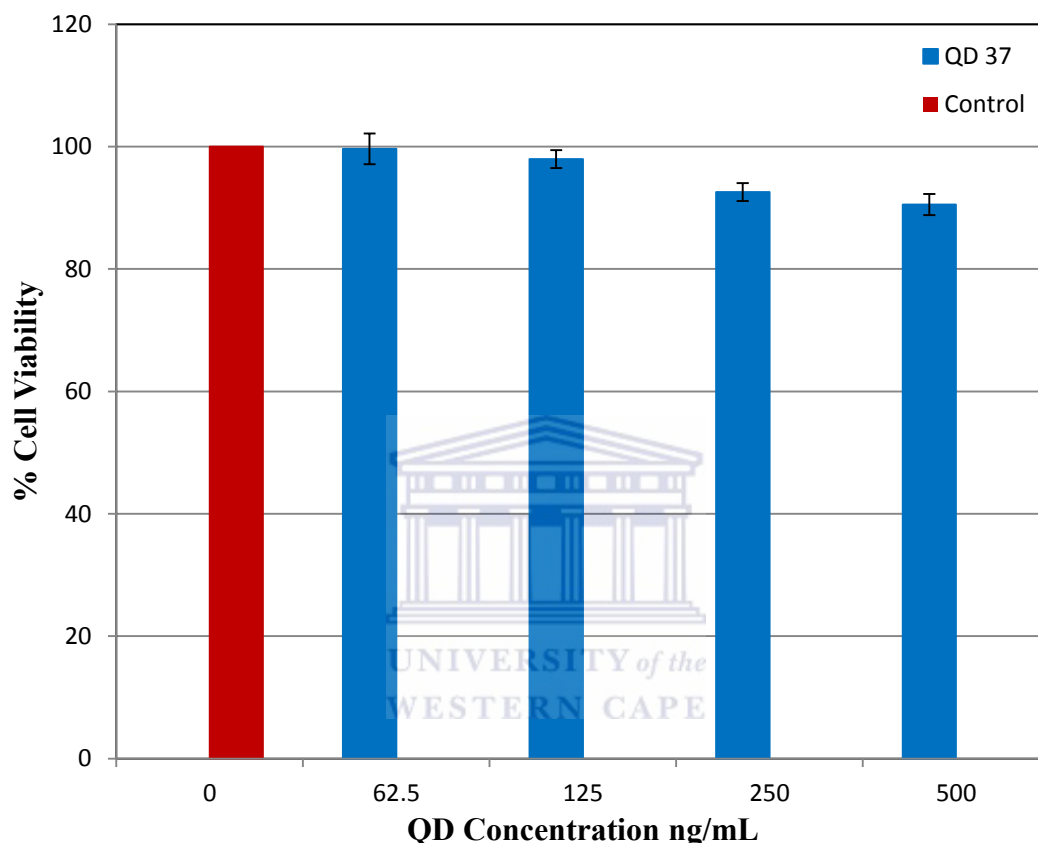


Figure 4.1 Effects of PbSe QDs on Caco-2 cell viability

Derfus *et al.* prepared mercaptoacetic acid-capped (MAA-capped) CdSe QDs and observed that they were not cytotoxic when the QDs were stored under inert atmosphere. They attributed QD toxicity to the oxidation of the surface by oxygen in air and ultraviolet (UV) light [5]. MUA used in this study has a longer carbon chain as compared to MAA and was expected to provide better passivation against photo-oxidation as discussed by Aldana *et al.* [7]. This in turn implies that QDs capped with longer chain mercaptocarboxylic acids are

likely to be less toxic than those with shorter chains since QD toxicity has largely been attributed to the release of heavy metal ions following their surface oxidation [8]. These results show that MUA-capped PbSe QDs could potentially be used as tools in disease diagnosis without harmful effects to cells.



4.2 References

- [1] Clift MJD, Stone V. Quantum dots: An insight and perspective of their biological interaction and how this relates to their relevance for clinical use. *Theranostics*, **2012**, 2, 668-680.
- [2] Ye L, Yong K, Liu L, Roy I, Hu R, Zhu J, Cai H, Law W, Liu J, Wang K, Liu J, Liu Y, Hu Y, Zhang X, Swihart MT, Prasad PN. A pilot study in non-human primates shows no adverse response to intravenous injection of quantum dots. *Nat. Nanotechnol.*, **2012**, 7, 453-458.
- [3] Hardman R. A toxicologic review of quantum dots: toxicity depends on physicochemical and environmental factors. *Environ. Health Persp.*, **2006**, 114, 165-172.
- [4] Tsoi KM, Dai Q, Alman BA, Chan WCW. Are quantum dots toxic? Exploring the discrepancy between cell culture and animal studies. *Accounts Chem. Res.*, **2013**, 46, 662-671.
- [5] Derfus AM, Chan WCW, Bhatia SN. Probing the cytotoxicity of semiconductor quantum dots. *Nano Lett.*, **2004**, 4, 11-18.
- [6] Peng L, He M, Chen B, Wu Q, Zhang Z, Pang D, Zhu Y, Hu B. Cellular uptake, elimination and toxicity of CdSe/ZnS quantum dots in HepG2 cells. *Biomaterials*, **2013**, 34, 9545-9558.
- [7] Aldana J, Wang A, Peng X. Photochemical instability of CdSe nanocrystals coated by hydrophilic thiols. *J. Am. Chem. Soc.*, **2001**, 123, 8844-8850.
- [8] Gomes SAO, Vieira CS, Almeida DB, Santos-Mallet JR, Menna-Barreto RFS, Cesar CL, Feder D. CdTe and CdSe quantum dots cytotoxicity: A comparative study on microorganisms. *Sensors*, **2011**, 11, 11664-11678.

5 Conclusions and recommendations

5.1 Conclusions

In this work, PbSe quantum dots with different capping agents were synthesized and characterized. Lead oxide and lead acetate were used for synthesis with lead oxide producing spherical QDs while lead acetate produced predominantly cubic quantum dots. PbSe QDs were synthesized following the organometallic and aqueous synthetic routes based on previously reported procedures [1,2]. All the organometallic and aqueous synthesised QDs had near-infrared emissions which were within the NIR biological window in which tissue absorbance and autofluorescence is minimal [3].

The effects of different parameters on the optical and structural properties of PbSe QDs were investigated using the organometallic synthetic route and it was observed that indeed the shapes and sizes of PbSe QDs can be varied by varying the reaction conditions. Most of the synthesized nanocrystals were spherical with diameters less than 10 nm. Higher temperatures were observed to result in faster QD growth as compared to lower reaction temperatures. Lower temperatures were also observed to produce a more homogenous distribution of QDs than higher temperatures as seen from their lower FWHM values. The source of selenium in the reaction was also observed to affect the size distribution of the QDs with TOPSe resulting in larger QDs as compared to TBPSe. It can therefore be concluded that synthetic conditions do have a major effect on the growth of semiconductor nanocrystals.

All the synthesized nanocrystals provided emissions in the NIR region of the spectrum which makes them favourable for biological applications since it has been established that nearly

background free deep tissue imaging can be achieved in this region due to low background fluorescence from biological milieu providing high signal to noise ratios [4].

The synthesized QDs were successfully transferred into aqueous media following ligand exchange reactions with 11-mercaptoundecanoic acid. The emission spectrum observed after ligand exchange was very similar to the one observed from aqueous synthesized QDs with the spectrum presenting as a perfect Gaussian peak (**Section 3.2** and **Section 3.3.1**).

High resolution transmission electron microscopy was used to provide an insight into the crystallinity of the QDs by showing the lattice fringes in the PbSe QDs. X-ray diffraction and selected area electron diffraction (SAED) patterns were used to confirm the crystal structure of PbSe nanocrystals which was found to be rock-salt cubic structure consistent with bulk PbSe.

The cytotoxicity of the synthesized PbSe quantum dots was investigated following the water-soluble tetrazolium salt (WST-1) assay using Caco-2 cells. The QDs were found to be non-toxic at all the tested concentrations with the highest tested concentration of 500 ng/mL resulting in approximately 90 % viability.

5.2 Recommendations

Lead based QDs provide near-infrared (NIR) fluorescence which is favourable for imaging applications because they can offer deep photon penetration [5]. The challenge currently facing near infrared imaging is the unavailability of the required instrumentation. Most of the available instruments are only able to monitor wavelengths and provide information in the ultra-violet (UV) and visible regions of the spectrum. The acquisition of instruments which are able to provide information on materials that emit within this region will greatly assist in the in depth study of their properties.

This study was dubbed a model study since it serves to pave way into the application of PbSe QDs as diagnostic tools by investigating their properties and cytotoxicity. Their near-infrared emission makes them superior fluorophores to the widely investigated CdSe QDs for imaging applications.

In future more studies should be carried out in order to establish the *in vitro* and *in vivo* stability of PbSe QDs. The effect of surface oxidation on the cytotoxicity of PbSe QDs should also be established. The mechanism of QD clearance from the body should be studied to provide an insight into the potential of QDs as new fluorescent agents. Future work should also be extended to study the applications of PbSe QDs as therapeutic or theranostic agents.



5.3 References

- [1] Primera-Pedrozo OM, Arslan Z, Rasulev B, Leszczynski J, Room temperature synthesis of PbSe quantum dots in aqueous solution: stabilization by interactions with ligands. *Nanoscale*, **2012**, 4, 1312-1320.
- [2] Stouwdam JW, Shan J, van Veggel FCJM, Pattantyus-Abraham AG, Young JF, Raudsepp M. Photostability of colloidal PbSe and PbSe/PbS core/shell nanocrystals in solution and in the solid state. *J. Phys. Chem. C.*, **2007**, 111, 1086-1092.
- [3] Smith AM, Mancini MC, Nie S. Second window for in vivo imaging. *Nat Nanotechnol.*, **2009**, 4, 710–711.
- [4] Amiot CL, Xu S, Liang S, Pan L, Zhao JX. Near-Infrared Fluorescent Materials for Sensing of Biological Targets. *Sensors*, **2008**, 8, 3082-3105.
- [5] Cassette E, Helle M, Bezdetnaya L, Marchal F, Dubertret B, Pons T. Design of new quantum dot materials for deep tissue infrared imaging. *Adv. Drug Deliv. Rev.*, **2013**, 65, 719-731.